

Dependences of Type Ia Supernovae Lightcurve Parameters on the Host Galaxy Star Formation Rate and Metallicity

Kohki Konishi^{1,2}, David Cinabro³, Peter M. Garnavich⁴, Yutaka Ihara⁵, Richard Kessler^{6,7}, John Marriner⁸, Donald P. Schneider⁹, Mathew Smith¹⁰, Harold Spinka¹¹, J. Craig Wheeler¹², Naoki Yasuda^{2,13}

kohki@icrr.u-tokyo.ac.jp

ABSTRACT

We present the dependences of the properties of type Ia Supernovae (SNe Ia) on their host galaxies by analyzing the multi-band lightcurves of 118 spectroscopically confirmed SNe Ia observed by the Sloan Digital Sky Survey (SDSS) Supernova Survey and the spectra of their host galaxies. We derive the equivalent width of the H α emission line, star formation rate, and gas-phase metallicity

¹Institute for Cosmic Ray Research, 5-1-5 Kashiwa-no-ha, Chiba, Japan

²Department of Physics, Graduate School of Science, University of Tokyo, Tokyo 113-0033, Japan

³Department of Physics and Astronomy, Wayne State University, Detroit, MI 48202 USA

⁴University of Notre Dame, 225 Nieuwland Science Hall, Notre Dame, IN 46556, USA

⁵Institute of Astronomy, Graduate School of Science, University of Tokyo, 2-21-1 Osawa, Mitaka, Tokyo 181-0015, Japan

⁶Kavli Institute for Cosmological Physics, The University of Chicago, 5640 South Ellis Avenue, Chicago, IL 60637, USA.

⁷Department of Astronomy and Astrophysics, The University of Chicago, 5640 South Ellis Avenue, Chicago, IL 60637, USA.

⁸Center for Particle Astrophysics, Fermi National Accelerator Laboratory, Batavia, IL 60510, USA

⁹Department of Astronomy and Astrophysics, 525 Davey Laboratory, Pennsylvania State University, University Park, PA 16802, USA.

¹⁰Astrophysics, Cosmology and Gravity Centre (ACGC), Department of Mathematics and Applied Mathematics, University of Cape Town, Rondebosch 7701, Cape Town, South Africa

¹¹Argonne National Laboratory, 9700 S. Cass Avenue, Lemont, IL 60437

¹²Astronomy Department, University of Texas, Austin, TX 78712, USA

¹³Institute for the Physics and Mathematics of the Universe, University of Tokyo, Kashiwa 277-8582, Japan

from the spectra and compare these with the lightcurve widths and colors of SNe Ia. In addition, we compare host properties with the deviation of the observed distance modulus corrected for lightcurve parameters from the distance modulus determined by the best fit cosmological parameters. This allows us to investigate uncorrected systematic effects in the magnitude standardization. We find that SNe Ia in host galaxies with a higher star formation rate have synthesized on average a larger ^{56}Ni mass and show wider lightcurves. The ^{56}Ni mass dependence on metallicity is consistent with a prediction of Timmes, Brown & Truran (2003) based on nucleosynthesis. SNe Ia in metal-rich galaxies ($\log_{10}(\text{O}/\text{H})+12 > 8.9$) have become 0.13 ± 0.06 magnitude brighter after corrections for their lightcurve widths and colors, which corresponds to up to 6 % uncertainty in the luminosity distance. We investigate whether parameters for standardizing SN Ia maximum magnitude differ among samples with different host characteristics. The coefficient of the color term is larger by 0.67 ± 0.19 for SNe Ia in metal-poor hosts than those in metal-rich hosts when no color cuts are imposed.

Subject headings: galaxies: abundances - galaxies: fundamental parameters - supernovae: general - surveys

1. Introduction

Type Ia Supernovae (SNe Ia) show diversity in their optical properties. The range of B-band peak luminosity is more than a factor of two. A series of lightcurve widths and colors have been demonstrated (Phillips 1993; Phillips et al. 1999; Tripp 1998). The radioactive element ^{56}Ni is explosively synthesized by the nuclear fusion of carbon and oxygen in SN Ia progenitors (Truran et al. 1967; Colgate & McKee 1969; Hillebrandt & Niemeyer 2000). The radioactive decay of this element is the major source of the SN Ia luminosity. For a decade there have been investigations of the link between the properties of SNe Ia and the galaxies which host these SNe Ia (e.g. Hamuy et al. 2000; Gallagher et al. 2005; Howell et al. 2009).

Hamuy et al. (2000) used 44 nearby SNe Ia and their hosts to claim that bright SNe Ia occur preferentially in young stellar environments by examining the trend between the decline rate of luminosity and the color (B-V) of their hosts. They also claimed that bright SNe Ia occur in low luminosity hosts by the examination of the luminosity decline rate and the host V-band magnitude. Gallagher et al. (2005) showed a tentative trend of fainter SNe Ia for metal-rich hosts. The star formation activity and metallicity of SN Ia host galaxies may also affect lightcurve properties of SNe Ia. These findings, however, have a large uncertainty due

to an insufficient sample size and should be updated with a larger set of data. Recently there has been a focus on the ^{56}Ni mass. Howell et al. (2009) and Neill et al. (2009) used over 100 pairs of SNe Ia and their host photometry to examine the dependence of the synthesized ^{56}Ni mass on stellar metallicity. If it can be assumed, as has been done by previous researchers, that when a host galaxy is metal-rich, a SN Ia progenitor in the galaxy is also metal-rich, one can link SN Ia characteristics with their progenitors. There is a theoretical prediction based on the nucleosynthesis: the mass of ^{56}Ni , a doubly-magic nucleus, becomes smaller and SN luminosity is lowered for SN Ia progenitors with larger metallicity, because of a larger fraction of neutron-rich nuclei ^{22}Ne (Timmer, Brown & Truran 2003). This prediction was suggested by an analytic model and supported by detailed simulations (Travaglio et al. 2005; Röpke et al. 2006). Observations have been consistent with this predictions (Howell et al. 2009; Neill et al. 2009).

SNe Ia are one of the best cosmological standard candles (e.g. Riess et al. 1998; Perlmutter et al. 1999). Considerable effort has been put into the standardization of maximum luminosity. Lightcurve properties such as stretch and color have been used to determine cosmological parameters (e.g. Kowalski et al. 2008; Kessler et al. 2009; Hicken et al. 2009). Recent studies (Sullivan et al. 2010; Kelly et al. 2010; Lampeitl et al. 2010b) reported that SNe Ia are brighter in massive hosts and hosts with low star formation rate (SFR) per stellar mass (specific SFR), after SN Ia maximum brightness have been corrected using their lightcurve shape and color. These results suggest host properties such as the host stellar mass can be treated as well as stretch and color to estimate a distance modulus (Guy et al. 2010). A recent simulation also suggests the possibility of systematic dependence of SN brightness on the progenitor metallicity (Kasen, Röpke & Woosley 2009).

Several studies have been conducted to investigate lightcurve properties and their dependences on their host properties for nearby and high- z SNe Ia. However, nearby samples tend to be biased toward luminous hosts, while high- z host spectra have yet to been investigated. The Sloan Digital Sky Survey (SDSS) -II Supernova Survey (Frieman et al. 2008) has performed a three year observation and spectroscopically confirmed 512 SNe Ia in the intermediate redshift range $0.05 < z < 0.4$. Around 20 % of SN Ia host galaxies were observed spectroscopically by the SDSS (York et al. 2000). With these data, we present relations between SN Ia lightcurve and their host gas properties. The dependences of the ^{56}Ni mass and the Hubble residuals are also presented. The data are presented in §2. The determination of host gas properties, ^{56}Ni masses, and the Hubble residuals are described in §3, and the sample for analysis is defined in §4. We present the results in §5, related discussion in §6 and the conclusions in §7. The adopted solar abundance is $\log_{10}(\text{O}/\text{H})+12 = 8.66$ from Asplund, Grevesse & Sauval (2005). We also adopt $\Omega_M = 0.281$, derived from only the SDSS-II first year cosmology sample under a spatially flat cosmological model with

a constant dark energy equation of state parameter (a sample for the spatially flat cosmological model with constant dark energy equation of state parameter; in Kessler et al. (2009)). The Hubble parameter is set to be $H_0 = 72 \text{ km sec}^{-1}\text{Mpc}^{-1}$.

2. Data

The SDSS-II Supernova Survey (Frieman et al. 2008; Sako et al. 2008) identified 512 spectroscopically confirmed SNe Ia at $0.05 < z < 0.4$, with lightcurves in five (*ugriz*; Fukugita et al. (1996)) bands from the SDSS 2.5m telescope (Gunn et al. 2006) and camera (Gunn et al. 1998). The survey area is Stripe 82, the 300 deg² southern equatorial stripe of the SDSS footprint, 20 h to 4 h in right ascension and -1.25 ° to +1.25 ° in declination. Figure 1a shows the redshift distribution for confirmed SNe Ia (dashed line), those with galaxy spectra (dotted line), and those plus good lightcurves (solid line, see also §5.2). The photon contribution from the galaxy component has been subtracted via the scene modeling photometry method (Holtzman et al. 2008). The sensitivities of the *u* and *z* filters are considerably lower than those of the *gri* bands, so our lightcurve analysis is restricted to the *gri* bands.

An important aspect of the SDSS-II Supernova Survey is that a larger fraction of SN Ia host galaxies were observed spectroscopically than SNe Ia discovered by other rolling search surveys. Spectroscopic observations were performed with the fiber spectrograph mounted on the SDSS 2.5m telescope. The fiber aperture was 3 arcsec in diameter and the fiber positions were selected to obtain spectra centered on galaxy cores. See Stoughton et al. (2002) for a description of the SDSS galaxy targeting and algorithm. The spectral coverage is 3800 to 9200 Å and the wavelength bin is set to 69 km sec⁻¹ per pixel in a log-lambda scale; the instrumental resolution is 1850 – 2200.

In order to identify SN Ia host galaxies, a search was conducted in the SDSS galaxy catalog for the closest one in isophotal radius using an exponential profile for the galaxy light. Based on comparing redshifts of host galaxies with the redshifts of spectroscopically identified SNe Ia, we estimate that the probability of a SN Ia not being properly matched with its galaxy host at less than a few percent. As a result of the SN-galaxy matching, we have emission line fluxes for 118 host galaxies. The redshift distribution of the sample is presented in Figure 1a (thin dashed line).

In order to examine environmental properties on SNe Ia, we used the emission line

flux measurements¹ by the MPA/JHU group available to the public. Their spectral sample includes: objects brighter than Petrosian $r = 17.77$ in the Data Release 7 (Abazajian et al. 2009) with (i) SPECTROTYPE = TARGETTYPE = 'GALAXY', a redshift less than 0.7 and a median signal-to-noise ratio (S/N) per pixel larger than zero for a sky-subtracted spectrum. The sky flux was occasionally over-subtracted 1-2 % and S/N can be below zero (Jarle Brinchmann; private comm.), or (ii) SPECTROTYPE = 'GALAXY' if the redshift is larger than 0.7 and S/N per pixel larger than 2, or (iii) SPECTROTYPE = 'QSO'. They measured line fluxes as follows: stellar continuum spectra of several different ages and metallicities were generated by a population synthesis code (Charlot & Bruzual 2010 in prep). Then a χ^2 fit was performed to construct the best fit continuum for each galaxy spectrum. After subtracting the best fit continuum from the observed spectra, line fluxes were determined by fitting those lines with Gaussians simultaneously. We averaged line fluxes when a galaxy was observed more than once. Figure 2a is the histogram of the equivalent width (EW) of the H α emission line (EW H α) for our sample. The distribution of EW H α has its peak at the 10-30 Å bin. These measurements are used to derive star formation rate surface density (SFR SD, whose calculation is described in §3.2), and gas-phase metallicity. Two kinds of possible biases might be included for our sample, one of which arises in the targeting of SNe for spectroscopic confirmation, and the other in the selection for host spectra in SDSS-I.

In Figure 3, we show the characteristics of the interstellar matter (ISM) for SN Ia host galaxies. We plot 77 of 118 SN Ia hosts with (i) a S/N above two for the H β , [O III] λ 5008, H α and [N II] λ 6585 line, and (ii) a redshift greater than 0.04 to avoid the domination of galaxy core components (maximum fraction 20 %) by fiber aperture effects (Kewley & Ellison 2008). Over 170,000 field galaxy observations were placed in 0.1 bins in $\log_{10}([\text{N II}]\lambda 6585/\text{H}\alpha)$ and $\log_{10}([\text{O III}]\lambda 5008/\text{H}\beta)$, and the contours connected bins with approximately 100, 2500, 5000, 7500 and 10000 galaxies (black contours from outer to inner). SN Ia host galaxies are shown in red. This is a diagnostic plot used to separate star forming galaxies and AGN-activity dominated galaxies (e.g. Veilleux & Osterbrock 1987). The black dotted curve shows the demarcation between star forming galaxies (left bottom) and AGN-like galaxies (right top) from Kauffmann et al. (2003). Of 77 hosts, 54 galaxies are classified as star-forming galaxies and 23 as AGN-powered galaxies. Moreover all the SN Ia host galaxies have the [N II] λ 6585/H α above -1.65, the lower flux ratio of the stellar wind model (Hachisu, Kato & Nomoto 1996, discussed below). We do not correct for reddening in this plot, because the wavelengths of [N II] λ 6585 and H α as well as [O III] λ 5008 and H β have only small separations.

¹<http://www.mpa-garching.mpg.de/SDSS/DR7>

A non negligible fraction of SNe Ia are observed in the outskirts of galaxies (Bartunov et al. 2007; Yasuda & Fukugita 2010). The metallicity at SN Ia sites can be estimated by global galaxy luminosity and a metallicity gradient (Henry & Worthey 1999). Although progenitor characteristics for core-collapse SNe may be easily estimated from SN local site information (e.g. Boissier & Prantzos 2009), the estimation is more complicated for SNe Ia. Several studies have shown a wide range of the SN Ia delay-time, i.e. the time from the birth of a progenitor star to its explosion ($\lesssim 180\text{Myr}$; Aubourg et al. 2008) to near the cosmic time ($\gtrsim 2.4\text{Gyr}$; Brandt et al. 2010). For SNe Ia with a long-delay time, local measurements at SN sites are probably not representative of the progenitor system, since they have the ability to travel significant distances from their star forming regions due to galaxy random motion and differential rotation. The mean diameter containing 90 % of light using Petrosian flux is 6.3 arcsec for our sample, which is larger than the fiber aperture. Some fibers contain only the light around cores of galaxies, so measured values may not be representative of the global galaxy properties. It is expected that a spatial distribution of these quantities varies among galaxies. We use three galaxy characteristics averaged over the 3 arcsec aperture centered on galaxy cores, metallicity, SFR SD and EW H α for this study. This would be another source of bias. We include SNe Ia in AGN-like galaxies, following a former study of Gallagher et al. (2005).

3. Measurements

3.1. Balmer color excess

The ratio of H α and H β lines provides an estimate of the color excess in a host galaxy assuming a constant intrinsic flux ratio.

The extinction law $k(\lambda)$ is defined as

$$k(\lambda) = \frac{A(\lambda)}{E(B - V)}, \quad (1)$$

where $A(\lambda)$ is the extinction at the wavelength λ in magnitude and $E(B - V)$ is the color excess in the B - relative to the V -band. $R_V = A(V)/E(B - V) = 3.1$ is adopted for our Galaxy. The extinction is defined as

$$A(\lambda) = -2.5 \log_{10} \left(\frac{f(\lambda)}{f_0(\lambda)} \right), \quad (2)$$

where $f(\lambda)$ is the observed flux and $f_0(\lambda)$ is the intrinsic flux without extinction.

The difference in $k(\lambda)$ between λ_1 and λ_2 is

$$\begin{aligned} k_1 - k_2 &= \frac{A_1 - A_2}{E(B - V)} \\ &= -\frac{1.086}{E(B - V)} \ln \frac{f_1/f_2}{(f_1/f_2)_0}. \end{aligned} \quad (3)$$

In the case of Balmer lines, $k(\text{H}\alpha) - k(\text{H}\beta) = -1.161$ for our Galaxy (Calzetti, Kinney & Storchi-Bergmann 1994). There is evidence that this difference is applicable to other galaxies, since the Galactic extinction laws are almost indistinguishable for the Magellanic Clouds within optical wavelengths, $1.0 < 1/\lambda < 4.0 \mu\text{m}^{-1}$ (Gordon et al. 2003). Although it has been suggested that the ratio of total to selective extinction R_V is smaller for SN Ia host galaxies (e.g. Nobili & Goobar 2008), we assume that the extinction law of SN Ia hosts is consistent with that in our Galaxy by following Takanashi, Doi & Yasuda (2008). Intrinsic flux ratios of $f(\text{H}\alpha)/f(\text{H}\beta)$ are presented in Osterbrock (1989) for optically thin (Case A) and optically thick nebulae (Case B). Since optically thin nebulae contain only a small amount of gas and therefore are difficult to observe, we use the Case B scenario $f_{\text{int}}(\text{H}\alpha)/f_{\text{int}}(\text{H}\beta)$ of 2.88. The Balmer color excess $E(B - V)$ from Balmer lines is calculated as follows:

$$E(B - V) = 0.935 \ln \frac{f_{\text{obs}}(\text{H}\alpha)/f_{\text{obs}}(\text{H}\beta)}{2.88}. \quad (4)$$

The uncertainties are propagated in quadrature. We assume the dust properties to be like those in our Galaxy and estimate $E(B - V)$ unless the S/N of both line fluxes are below 2 (“N/A” is tagged for non detection and “—” for low S/N cases in Table 1). The spectra are corrected for the reddening of their Balmer color excess.

3.2. Star formation rate

We calibrate the SFR from the $\text{H}\alpha$ line, since it is a direct tracer of young stellar populations given by Kennicutt (1998)

$$\text{SFR}(\text{M}_\odot \text{ yr}^{-1}) = 7.9 \times 10^{-42} L(\text{H}\alpha)(\text{erg sec}^{-1}), \quad (5)$$

where $L(\text{H}\alpha)$ is the $\text{H}\alpha$ luminosity in the galaxy rest frame.

We also estimated the SFR SD by normalizing the SFR by its physical area, which is defined as a circle corresponding to the fiber aperture for the SDSS spectra. Figure 2b is the histogram of SFR SD for our sample. The distribution of SFR SD has its peak in the bin of 0.1 to 0.3 $\text{M}_\odot \text{ yr}^{-1} \text{ kpc}^{-2}$. Table 1 lists the results. “N/A” is tagged for non-emission galaxies and “—” for low S/N cases.

3.3. Metallicity

Oxygen is the most abundant metal in the gas-phase, only weakly depleted, and exhibits very strong forbidden lines in the optical wavelength range. Ideally, the metallicity is measured from the gas temperature and derived from the flux ratio of the [O III] λ 4364 line to the [O III] λ 5008 line. However, it can apply only for metal-poor galaxies, since the [O III] λ 4364 line, an auroral line, becomes invisible under metal-rich and cooled environments. Another method is the usage of strong line ratios. We use the latter method by following the description of Kewley & Dopita (2002, hereafter KD02), which is reviewed.

KD02 suggests using the flux ratio of $R = [\text{N II}]\lambda 6585 / [\text{O II}]\lambda 3727$, where [O II] λ 3727 is an abbreviated form of [O II] $\lambda\lambda$ 3726,3729. This ratio increases strongly with increasing metallicity for two reasons. First, since nitrogen is predominantly a secondary stellar nucleosynthesis element while oxygen is a primary one, the [N II] production is roughly proportional to pre-existing seed [O II]. Second, the excitation energy of the electron-ion collision is higher for [O II] λ 3727 than for [N II] λ 6585. In metal-rich environments, there are fewer thermal electrons with energy high enough to create the [O II] λ 3727 line. We use Equation 7 of KD02 for the metallicity calibration

$$\log_{10}(O/H) + 12 = \log_{10}(1.54020 + 1.26602R + 0.167977R^2) + 8.93. \quad (6)$$

If the metallicity is above $0.4Z_{\odot}$, KD02 suggests that the derived metallicity is taken as a final estimate. We tagged these galaxies for which this calibration is used as “N2/O2a”, “N2/O2d” or “N2/O2g” in the column 7 of Table 1; “a” is attached for the galaxies with the detection of [O II], H β , [O III], [N II] and [S II], “d” for those with [O II], H β , [O III] and [N II], “g” for those with only [O II] and [N II]. The R value is corrected based on the reddening correction of the Balmer line ratio.

$R_{23} = ([\text{O II}]\lambda 3727 + [\text{O III}]\lambda\lambda 4959, 5008) / \text{H}\beta$ is also dependent on metallicity, for oxygen is one of the principal nebular coolants. The caveat for this indicator is that the calibration coefficients are model dependent. Several authors have proposed theoretical calibration schemes, including common ones by McGaugh (1991), Zaritsky, Kennicutt & Huchra (1994), Charlot & Longhetti (2001) and Kobulnicky & Kewley (2004) (hereafter M91, Z94, C01 and KK04, respectively). The limitation of the R_{23} ratio is that it gives two values of metallicity (shown *upper* and *lower* in Equation 7a). Since KD02 claimed that R values are more effectively related to metallicity at high metallicities than R_{23} , they suggested to use R for their high values ($> 0.5 Z_{\odot}$) and R_{23} for small values ($< 0.5 Z_{\odot}$).

M91 examined the behavior of R_{23} with metallicity by including the effects of dust and variation in ionization parameter when modelling H II regions. We use the analytic expression

of M91 given in Kobulnicky, Kennicutt & Pizagno (1999) to calibrate the metallicity

$$[\log_{10}(O/H) + 12]_{upper} = 12.0 - 2.939 - 0.2x - 0.237x^2 - 0.305x^3 - 0.0283x^4 - y(0.047 - 0.0221x - 0.102x^2 - 0.0817x^3 - 0.00717x^4) \quad (7a)$$

$$[\log_{10}(O/H) + 12]_{lower} = 12.0 - 4.944 + 0.767x + 0.602x^2 - y(0.29 + 0.332x - 0.331x^2), \quad (7b)$$

where $x = \log_{10} R_{23}$ and

$$y = \log_{10} \left(\frac{[O \text{ III}] \lambda \lambda 4959, 5008}{[O \text{ II}] \lambda 3727} \right). \quad (8)$$

Z94 reported that an average of the three calibrations by Edmunds & Pagel (1984), McCall, Rybski & Shields (1985) and Dopita & Evans (1986) yields:

$$\log_{10}(O/H) + 12 = 9.265 - 0.33R_{23} - 0.202R_{23}^2 - 0.207R_{23}^3 - 0.333R_{23}^4. \quad (9)$$

C01 presents a number of calibrations for various available lines. Their calibrations are based on a combination of stellar population synthesis and photoionization codes with a simple model for the dust. One of their formulae, also used in KD02, provides the following metallicity relation:

$$\log_{10}(O/H) + 12 = \log_{10} \left[5.09 \times 10^{-4} \left(\frac{[O \text{ II}]/[O \text{ III}]}{1.5} \right)^{0.17} \left(\frac{[N \text{ II}]/[S \text{ II}]}{0.85} \right)^{1.17} \right] + 12. \quad (10)$$

KD02 provide a number of calibrations based upon the availability of particular nebular emission lines. KK04 advocate an iterative approach to solve for both quantities

$$[\log_{10}(O/H) + 12]_{upper} = 9.72 - 0.777x - 0.951x^2 - 0.072x^3 - 0.811x^4 - \log_{10}(q)(0.0737 - 0.0713x - 0.141x^2 - 0.0373x^3 - 0.058x^4) \quad (11a)$$

$$[\log_{10}(O/H) + 12]_{lower} = 9.40 + 4.65x - 3.17x^2 - \log_{10}(q)(0.272 + 0.547x - 0.513x^2). \quad (11b)$$

where q is the ionization parameter, determined from

$$\log_{10}(q) = \{32.81 - 1.153y^2 + [\log_{10}(O/H) + 12](-3.396 - 0.025y + 0.1444y^2)\} \times \{4.603 - 0.3119y - 0.163y^2 + [\log_{10}(O/H) + 12](-0.48 + 0.0271y + 0.02037y^2)\}^{-1}. \quad (12)$$

KD02 compared various calibrations and presented an empirical calibration scheme for metallicity over a wide range. For the galaxies with estimated metallicity below $0.5Z_{\odot}$ from

Equation 6, the average of the M91 formula (Equation 7a) and Z94 formula should be taken (Equation 9). If the value is above $0.4Z_{\odot}$, the derived metallicity is the final estimate. The symbol “1b” is tagged to such galaxies with $> 0.4Z_{\odot}$ in the column 7 of Table 1. For the galaxies with estimated metallicity below $0.5Z_{\odot}$, the average of the C01 formula (Equation 10) and KK04 formula (Equation 11b) should be taken if they have [O II], H β , [O III], [N II] and [S II] measurements; these galaxies are tagged with “1c”. The Z94 formula (Equation 9) should be used for the galaxies with these three emission lines [O II], H β and [O III] (tagged as “3f”). The metallicity for 102 of 118 SN Ia hosts are derived; the remaining 16 hosts either have only H α (and H β) emission line (tagged as “CaseX”) or no lines above S/N > 2 (tagged as “N/A”). Figure 2c is the histogram of metallicity for our sample. The distribution of metallicity has its peak in the 9.0 to 9.2 bin. This might result from the spectroscopic target selection by the SDSS-I Legacy survey where only galaxies brighter than $r = 17.77$ mag were selected. Bright galaxies have already grown up to be massive and metal-rich in the nearby Universe (e.g. Tremonti et al. 2004). Table 1 summarizes the spectroscopic properties for the host galaxy spectra. The uncertainty in metallicity is calculated by the propagation of uncertainties in line flux measurements.

3.4. Ejected ^{56}Ni mass

Theoretical prediction The main source of SN luminosity is the decay of the synthesized radioactive ^{56}Ni (Truran et al. (1967), Colgate & McKee (1969)). Brighter SNe presumably possess larger ^{56}Ni mass. Timmes, Brown & Truran (2003) proposed that less ^{56}Ni mass is created from metal-rich progenitors from their models that conserved charge and mass at the explosion: the fusion of ^{12}C and ^{16}O triggers the detonation that produces ^{56}Ni , ^{58}Ni and ^{54}Fe . The electron-to-nucleon ratio and mass fraction after the explosion are

$$Y_e = \frac{Z(^{56}\text{Ni})X(^{56}\text{Ni})}{A(^{56}\text{Ni})} + \frac{Z(^{58}\text{Ni})X(^{58}\text{Ni})}{A(^{58}\text{Ni})} \quad (13)$$

$$X(^{56}\text{Ni}) + X(^{58}\text{Ni}) = 1. \quad (14)$$

Here $Z(i)$ and $A(i)$ are the number of protons and nucleons (protons plus neutrons) of the element i , respectively, and $X(i)$ is the mass fraction. The relation between the ^{56}Ni mass and the electron-to-neutron ratio is thus

$$M(^{56}\text{Ni}) = 0.6X(^{56}\text{Ni}) = 0.6(58Y_e - 28), \quad (15)$$

where a typical ^{56}Ni mass for the $Y_e = 0.5$ progenitor is set to be $0.6 M_{\odot}$. $X(^{54}\text{Fe})$ was set to be zero for simplification. Inclusion of this element makes the slope of Y_e vs. $M(^{56}\text{Ni})$ shallower by a factor of $(58 - 56.8)/58 \sim 2\%$.

Estimate of Y_e In order to derive the ^{56}Ni mass, a straight-forward method is to measure the abundance of SN Ia progenitors. However, this measurement is difficult, since we observe the results of element synthesis in SNe Ia. The best current effort is to use the metallicity of their hosts. With the definition of the electron-to-nucleon ratio Y_e and the formula of the mass fraction for CO white dwarfs $\sum X(i) = 1$, Y_e is expressed as follows (Howell et al. 2009):

$$\begin{aligned} Y_e &= \frac{6}{12}X(^{12}\text{C}) + \frac{8}{16}X(^{16}\text{O}) + \frac{10}{22}X(^{22}\text{Ne}) + \frac{26}{56}X(^{56}\text{Fe}) \\ &= \frac{1}{2} - \left\{ X(\text{H}) \left(\frac{\text{Fe}}{\text{H}} \right) \left(3 + \left(\frac{\text{C}}{\text{Fe}} \right) \right) + X(\text{H}) \left(\frac{\text{O}}{\text{H}} \right) \left(2 + \left(\frac{\text{N}}{\text{O}} \right) \right) \right\}. \end{aligned} \quad (16)$$

We assume a constant (C/Fe) in our metallicity range (Wheeler, Sneden & Truran 1989) and set X(H) and (C/Fe) to be the solar values of 0.7392 and 8.7 (Asplund, Grevesse & Sauval 2005). From observations of nearby galaxies or stars within our Galaxy, (N/O) and (Fe/H) increase with (O/H) (e.g. Pagel & Edmunds 1981; Wheeler, Sneden & Truran 1989). We take the dependence of (O/H) on (N/O) from Vila-Costas & Edmunds (1993): (N/O) = 0.0316 + 126 (O/H) and on (Fe/H) from Ramirez, Prieto & Lambert (2007):

$$\left(\frac{\text{Fe}}{\text{H}} \right) = 10^{-a/(1+b)} \frac{(\text{Fe}/\text{H})_{\odot}}{(\text{O}/\text{H})_{\odot}^{1/(1+b)}} \left(\frac{\text{O}}{\text{H}} \right)^{1/(1+b)}, \quad (17)$$

where $a = 0.096$ and $b = -0.327$ for the thin disk. Solar oxygen and iron abundances are derived from Asplund, Grevesse & Sauval (2005): $\log_{10}(\text{O}/\text{H})_{\odot} = -3.34$ and $\log_{10}(\text{Fe}/\text{H})_{\odot} = -4.55$. From Equations 16 and 17, the ^{56}Ni mass is represented by a function of (O/H) with four coefficients. It decreases with increasing metallicity.

Prior to the explosion, electron capture by ^{12}C burning (simmering) can reduce the free electron abundance and therefore reduce the amount of synthesized ^{56}Ni . The effect of electron capture on the variation of ^{56}Ni mass may be small $\lesssim 5\%$ (Chamulak et al. 2008). We ignore this simmering effect. Although the far UV flux varies with Fe abundance, we can neglect this impact on the ^{56}Ni mass, since the flux would only be $\sim 3 \times 10^{-3}$ times larger than the optical flux (Sauer et al. 2008).

Estimate of ^{56}Ni mass We now describe the method to obtain the ^{56}Ni mass from SN Ia lightcurves. Since the radioactive decay of ^{56}Ni powers the SN Ia luminosity (Truran et al. (1967); Colgate & McKee (1969)) mainly for the photospheric phase, the maximum bolometric luminosity L_{bol} is comparable to the radioactive luminosity. The ^{56}Ni mass is well described by

$$M(^{56}\text{Ni}) = \frac{L_{bol}}{\gamma \dot{S}(t_R)}, \quad (18)$$

where $\dot{S}(t_R)$ is the radioactive luminosity per solar mass of ^{56}Ni and γ is the ratio of bolometric to radioactive luminosity (Arnett 1982).

Multi-band lightcurves are used to estimate the bolometric luminosity. We first derive the lightcurve parameters using the SALT2 lightcurve fitting code (Guy et al. 2007). The SALT2 code employs a two-dimensional spectral surface $F(p, \lambda)$ in time and wavelength constructed by the average temporal evolution of the spectral energy distribution for SNe Ia (M_0) and its deviation (M_1).

$$F(p, \lambda) = x_0 \times [M_0(p, \lambda) + x_1 M_1(p, \lambda)] \times \exp[c_{salt} CL(\lambda)], \quad (19)$$

where p is the rest-frame days from the date of peak luminosity, x_0 is the normalization, and x_1 is the coefficient corresponding to the lightcurve width. $CL(\lambda)$ is the average color correction law and c_{salt} is its coefficient, which is sensitive to both intrinsic color diversity and the host-dust reddening. The SALT2 fit returns lightcurve parameters (x_0, x_1, c_{salt}) for each SN Ia.

Wang et al. (2009) presented an extensive dataset of a normal SN Ia (SN 2005cf) from UV to near infrared wavelengths. Since the UV flux variation is not fully understood (Höflich, Wheeler & Thielemann 1998; Lentz et al. 2000; Sauer et al. 2008), we assume a negligible variation of UV flux among SNe Ia and adopt 0.30 for the fraction of missing flux outside the optical window from 2900 to 7000 Å (their Figure 24). The maximum bolometric flux can thus be estimated using lightcurve parameters, spectral surfaces, and the luminosity distance d_L ,

$$L_{bol} = \frac{4\pi d_L^2}{1 - 0.30} \int_{2900}^{7000} F(0, \lambda) d\lambda. \quad (20)$$

The radioactive luminosity per solar mass of ^{56}Ni can be estimated using e -folding decay times for $^{56}\text{Ni} \rightarrow ^{56}\text{Co}$ and $^{56}\text{Co} \rightarrow ^{56}\text{Fe}$ of 8.8 and 111 days, and mean energy release per decay of 1.71 and 3.76 MeV,

$$\begin{aligned} \dot{S} &= 6.31 \times 10^{43} e^{-t_R/8.8} \\ &+ 1.43 \times 10^{43} e^{-t_R/111} \text{erg sec}^{-1} M_\odot^{-1}, \end{aligned} \quad (21)$$

where t_R is the time from the explosion to maximum B-band brightness (the rise time). The rise time is described by a 'stretch' parameter $s(B)$ which determines broadening or narrowing of an average template (Perlmutter et al. 1997; Guy et al. 2005). Following an average stretch-corrected rise time of 19.5 ± 0.2 days (Riess et al. 1999; Aldering et al. 2000; Goldhaber et al. 2001; Conley et al. 2006), we set $t_R/s(B) = 19.5$ (Howell et al. 2009). $s(B)$ is derived from the width x_1 and the polynomial calibration given in Guy et al. (2007)

². We have not tried to incorporate the variation in SN rise time reported by Hayden et al. (2010) or use their more precise rise time of 17.38 ± 0.17 . Our results are not sensitive to the exact value used, and we prefer to maintain a simple estimate of the ⁵⁶Ni mass based on the SALT2 light curve parameterization. The uncertainty in \dot{S} is derived from Equation 21,

$$\sigma_{\dot{S}}/\sigma_S = (1.40 \times 10^2 e^{-2.22s(B)} + 2.51 \times e^{-0.18s(B)}) \times 10^{42}. \quad (22)$$

The quantity γ is a correction factor between bolometric to radioactive luminosity. The peak luminosity is equal to the instantaneous rate of energy deposition by the ⁵⁶Ni decay assuming constant opacity with time (Arnett 1982). Since the opacity decreases with the temperature, thermal energy stored in opaque regions is released and adds to the luminosity at later phases i.e. $\gamma > 1$. There will be an intrinsic variance in a radial distribution of elements in SNe Ia and this could change the intrinsic variance of γ ³. γ is thought to be roughly 10 % (Branch & Khoklov 1995). We reflect the uncertainty of the intrinsic variance by assigning this ratio to be 1.2 ± 0.1 (Branch & Khoklov 1995; Howell et al. 2006, 2009).

Following the work of Howell et al. (2009), the uncertainty in the ⁵⁶Ni mass is derived by propagating uncertainties in the bolometric luminosity, the radioactive luminosity and the quantity γ ,

$$\sigma_{^{56}\text{Ni}} = \sqrt{\left(\frac{1}{\gamma\dot{S}}\right)^2 \sigma_{L_{bol}}^2 + \left(\frac{L_{bol}}{\gamma\dot{S}^2}\right)^2 \sigma_{\dot{S}}^2 + \left(\frac{L_{bol}}{\gamma\dot{S}^2}\right)^2 \sigma_{\gamma}^2}, \quad (23)$$

where σ_{γ} is set to 0.1.

3.5. Hubble residual

The Hubble residual (HR) is defined as the difference in these two distance moduli:

$$\mu_B^{corr} = \{m_B^*(x_0) + \alpha x_1 - \beta c_{salt}\} - \bar{M} \quad (24)$$

$$\mu_B^{bestfit} = 5 \log_{10} \left(\frac{d_L(z, \Omega_M, \Omega_{\Lambda})}{10pc} \right) \quad (25)$$

$$HR = \mu_B^{corr} - \mu_B^{bestfit}, \quad (26)$$

²The $s(B)$ parameter is produced directly by Perlmutter et al. (1997) or Guy et al. (2005). We believe that the SALT2 code represents SN Ia characteristics more realistically due to a larger training dataset.

³In case of SNe Ia with ⁵⁶Ni distributed toward the outer layer, photons deposited from the outer layer can easily escape and γ for such SNe Ia might be small.

where M is the average absolute magnitude of SNe Ia and m_B^* is the observed peak magnitude. The HR would be zero for a perfect standard candle, but in practice has an intrinsic scatter of ~ 0.15 mag. Various efforts have been made to reduce this scatter and randomize it at all redshifts (e.g. Phillips 1993; Riess, Press & Kirshner 1996; Guy et al. 2007; Jha, Riess & Kirshner 2007; Kessler et al. 2009).

We derive standardization parameters for luminosity α , β and M so that the $\chi^2 = \sum \left(\frac{HR^2}{(\delta\mu_B)^2 + \sigma_{int}^2} \right)$ is minimized for the parameters. The error in distance modulus $\delta\mu_B$ is calculated by the error propagation of the covariance matrix. The intrinsic dispersion σ_{int} is set to be 0.14 mag (Lampeitl et al. 2010b) and is added in quadrature to the error $\delta\mu_B$ to achieve a reduced χ^2 close to one (Lampeitl et al. 2010a). We use the three samples: SNe Ia with (i) host EW H α , (ii) host SFR SD, and (iii) metallicity.

4. Sample selection

We investigate the link between SN Ia lightcurve properties and their host properties. Since our lightcurves have been obtained by a period-determined survey, SNe Ia which were discovered near the beginning or the end of the period are incomplete. The following criteria for lightcurves were set for the analysis to examine SNe Ia whose lightcurves can be reconstructed accurately by the SALT2 fitter:

1. at least one data point with $p < -4$,
2. at least one data point with $p > +4$,
3. at least five data points with $-20 < p < +60$,
4. lightcurve parameters with $|x_1| < 5.0$ and/or $|c_{salt}| < 2.0$,

where p is the rest-frame phase in days. 30 of a total of 118 SNe Ia do not meet at least one of the criteria above, 23 of which do not meet the first three criteria, and five SNe Ia (SN 12897, 13610, 16644, 18835, 20420) do not meet the fourth criteria. The fourth criterion excludes an additional two SNe Ia which are known to have unusual lightcurves: SN2005hk (Phillips et al. 2007) and SN2007qd (McClelland et al. 2010).

Figure 1 shows the distributions of redshift (panel a), lightcurve widths (panel b) and colors (panel c) of SNe Ia. The bold dashed histograms are the distributions for 512 spectroscopically confirmed SNe Ia. The thin dashed histograms are those for the 118 with host galaxy spectra. The solid histograms are for the 86 passing the lightcurve criteria in addition

to having host spectra (the good LC sample). Arrows are the average width and color for confirmed SNe Ia (bold dashed; -0.04 ± 0.07 and 0.00 ± 0.01) and the good LC sample (bold solid; -0.49 ± 0.15 and 0.08 ± 0.02). The average values for the good LC sample are lower in x_1 and higher in c_{salt} . This may be because the confirmed sample contains intrinsically bright SNe Ia at high redshifts: the x_1 and c_{salt} distributions for the good LC sample and the confirmed SNe Ia in a similar redshift range ($z < 0.2$; the dotted histogram in the panel b) come from the same distribution with a 68% and 98 % probability, respectively. The best fit Gaussian to the color histogram of the good LC sample is $\propto \exp(-((c_{salt} - c_0)^2/2\sigma_c^2))$, where $c_0 = 0.030$ and $\sigma_c = 0.098$. This Gaussian is used to separate the dust-extinguished SNe Ia in §5.2.

In order to examine dependences of SN lightcurve properties on their hosts over a wide range of host properties, we use hosts with $EW(H\alpha)/\delta EW(H\alpha) > 1$ and $f(H\alpha)/\delta f(H\alpha) > 1$ for the EW $H\alpha$ and SFR SD sample. We divide each sample into sets of equal and sufficient numbers of SNe Ia from the highest value of EW $H\alpha$, SFR SD, or metallicity to examine average trends. The mean, the error on the mean, and the deviation (when necessary) for each set are shown as red points in §5.2 and §5.3. The average value at the left-most point results from the remaining SNe Ia.

5. Results

5.1. The ^{56}Ni mass

Figure 4 is the histogram of ^{56}Ni masses for our sample. The ^{56}Ni mass ranges from around $1.0 M_\odot$ to all the way down close to zero. The least ^{56}Ni mass was $0.036 M_\odot$ for SN12979. Note that, for SNe Ia with the ^{56}Ni mass less than $0.2 M_\odot$, all the SNe Ia show large c_{salt} ($\gtrsim 0.3$). It is likely that the ^{56}Ni mass were underestimated due to the dust extinction of their host galaxies. The only exception is a SN Ia with the ^{56}Ni mass of $0.06 M_\odot$. The low value is attributed to a small lightcurve width ($x_1 \sim 4.0$). The bolometric flux correction was assumed to be constant for each SN Ia. This correction is based on only one SN Ia spectrum (§3.4). The wide ^{56}Ni mass range, however, can not be explained by varying the correction factor. The range of the correction should be 0.76 (for SNe Ia with ^{56}Ni mass of $0.2 M_\odot$) or even negative (-0.16 for those of $1.0 M_\odot$) to match to a SN Ia with the ^{56}Ni mass of $0.6 M_\odot$. This scatter has a trend with decline rate (Phillips 1993) and $(B - V)$ color at maximum date (Tripp 1998). The left part of Figure 5 shows the color-corrected magnitude $m_B - \beta c - \mu_{best}$ against the width x_1 . The right part of Figure 5 shows the width-corrected magnitude $m_B + \alpha x_1 - \mu_{best}$ against the color c_{salt} . SNe Ia with the ^{56}Ni mass less than $0.3 M_\odot$ or more than $0.8 M_\odot$ are marked in large solid circles. The linear

lines in Figure 5 are derived by minimizing $\chi^2 = \sum \left(\frac{HR^2}{(\delta\mu_B)^2 + \sigma_{int}^2} \right)$. SNe Ia with small or large ^{56}Ni masses follow the overall trend. Kasen & Woosley (2007) explained these empirical relations as a temperature variation: in a cool system, the recombination of Fe III to Fe II and the development of numerous Fe II/Co II absorption lines become noticeable at earlier phases in the B band wavelength range. This results in a fast decline of SN Ia brightness. The number fraction of our sample is the highest in the ^{56}Ni mass range from $0.40 M_\odot$ to $0.65 M_\odot$.

Stritzinger et al. (2006) compared two methods for deriving the ^{56}Ni mass. One method is to obtain bolometric luminosity at maximum brightness with a constant γ . The other is to model Fe features in nebular phase spectra. All the masses except two out of a total of 17 are consistent within 20 %. Since nebular spectra of our SNe Ia can not be observed by current instruments, we have adopted the former method described in §3.4. This approach yielded a ^{56}Ni mass range from $0.1 M_\odot$ for a subluminous SN Ia (SN 1991bg) to $1.0 M_\odot$, a comparable mass range to our sample.

5.2. Environmental effects on lightcurve properties

We start with an investigation of relations among SN Ia lightcurves and host gas properties: width x_1 and color c_{salt} for SNe Ia, and EW $\text{H}\alpha$, SFR SD, and metallicity for their hosts. Figure 6 shows dependences of the lightcurve width x_1 on host gas properties: (a) EW $\text{H}\alpha$ for 74 SNe Ia, (b) SFR SD for 74 SNe Ia and (c) metallicity for 67 SNe Ia. The metallicity is represented as $\log_{10}(\text{O}/\text{H})+12$ (lower horizontal axis) or $[\text{Fe}/\text{H}]$ (upper horizontal axis) by Equation 17. Note that $[\text{Fe}/\text{H}]$ is negative for thin disk stars with $[\text{O}/\text{H}]=0$ (Ramirez, Prieto & Lambert 2007). The vertical dotted line indicates the value of solar metallicity. SN17332 with the lightcurve properties of $(x_1, c_{salt})=(-0.53, 0.11)$ is eliminated from the following metallicity dependence plots because its host metallicity is extremely low $\log_{10}(\text{O}/\text{H})+12=7.77$. The maximum x_1 appears to be independent of the host properties. However, from the data in Figures 6a and 6b it appears that the lower value decreases from -1.0 for SNe Ia in hosts with a large EW $\text{H}\alpha$ of around $10^{1.8}\text{\AA}$) or with high star formation rate (SFR SD value of $10^0 M_\odot \text{ yr}^{-1} \text{ kpc}^{-2}$), to -2.5 for those in hosts with a low EW $\text{H}\alpha$ of around 10^{-1}\AA or with low star formation rate (SFR SD value of $10^{-1.5} M_\odot \text{ yr}^{-1} \text{ kpc}^{-2}$). Moreover, the dispersion of x_1 for hosts with the low EW $\text{H}\alpha$ of the sample is 1.1, which is comparable to that for hosts with a high EW $\text{H}\alpha$. The Kolmogorov-Smirnov (KS) test gives the probabilities that SNe Ia in hosts with low and high EW $\text{H}\alpha$ come from the same population to be $< 1\%$. The same result is obtained for the SFR surface density. The lower value of x_1 appears to increase from -2.5 for SNe Ia in metal-rich ($\log_{10}(\text{O}/\text{H})+12$ value of

~ 9.3) hosts to -1.5 for those in metal-poor ($\log_{10}(\text{O}/\text{H})+12$ value of 8.6) hosts (Figure 6c), being the KS probability of 81 %.

Similarly, Figure 7 shows dependences of the color c_{salt} on host gas properties: (a) EW $\text{H}\alpha$, (b) SFR SD, and (c) metallicity. The c_{salt} range is essentially constant with respect to the EW $\text{H}\alpha$ of their hosts (Figure 7a). If the parameter c_{salt} were completely explained by host-dust reddening, it would show a correlation with SFR SD. Figure 7b shows wider c_{salt} values (-0.2 to 0.2) for SNe Ia in hosts with modest SFR ($\log_{10}(\text{SFR SD})$ of -1.5 to 0.5 $M_{\odot} \text{ yr}^{-1} \text{ kpc}^{-2}$) than those in high/low star forming hosts. Some SNe Ia with large c_{salt} ($\gtrsim 0.2$) occur in the hosts with low star forming (SFR SD below $10^{-1.5} M_{\odot} \text{ yr}^{-1} \text{ kpc}^{-2}$) or high metallicity above 9.0. From Figure 7c, it appears that the range of c_{salt} is wider (-0.2 to 0.2) for SNe Ia in metal-rich ($\log_{10}(\text{O}/\text{H})+12 > 9.0$) hosts than for those in metal-poor ($\log_{10}(\text{O}/\text{H})+12 < 8.6$) hosts, 0.0 to 0.1 , but a KS test shows that the two distributions are compatible at the current level of statistical accuracy.

The c_{salt} parameter measures SN reddening relative to the nominal SALT2 templates. SN reddening can be caused by host galaxy dust extinction, intrinsic variations in the SN explosion, its immediate environment or some mixture of them. A flat c_{salt} distribution irrespective of the SN radial position (Yasuda & Fukugita 2010) and a correlation of the pseudo equivalent width of the “Si II $\lambda 4130$ ” feature of a SN Ia spectrum with c_{salt} (Nordin et al. 2010) support that the intrinsic variation of the SN explosion is introduced in c_{salt} . We exclude SNe Ia with $c_{salt} > 0.3$, larger than 3σ deviation from the averaged color in our sample (Figure 1c), since those SNe are most likely reddened primarily by host galaxy extinction.

Since the ^{56}Ni mass synthesized in the SN explosion is estimated from their lightcurves, it is expected to have some dependence on their host properties. Moreover a metallicity dependence can be compared with a theoretical prediction. Figure 8 shows the dependences on (a) EW $\text{H}\alpha$, (b) SFR SD, and (c) metallicity. The upper values of the ^{56}Ni mass do not change with respect to these host properties. However, from the data in Figures 8a and 8b, it appears that the lower value decreases from $0.4 M_{\odot}$ for SNe Ia in hosts with a large EW $\text{H}\alpha$ and with high star formation rate, to $0.2 M_{\odot}$ for those in hosts with a low EW $\text{H}\alpha$ or with low star formation rate. The lower value of the ^{56}Ni mass appears to increase from $0.25 M_{\odot}$ for SNe Ia in metal-rich hosts to $0.4 M_{\odot}$ for those in metal-poor hosts (Figure 8c). The KS test gives the probabilities that SNe Ia in hosts with low and high star formation rate (EW $\text{H}\alpha$, metallicity) come from the same population to be 12 % (38 %, 84 %). This indicates that the amount of the ^{56}Ni mass is the most sensitive to the young star fraction of their hosts. Five averaged points show that the ^{56}Ni mass is constant below $\log_{10}(\text{O}/\text{H})+12 < 8.9$ and that it decreases towards high-metal hosts. The average ^{56}Ni mass in the highest

metallicity bin is $\sim 0.11 M_{\odot}$ smaller than those in the two lowest metallicity bins (but only at $\sim 1.6\sigma$). A similar trend appears when we divide the dataset into five equally-spaced bins (0.16 dex) or when we make six representative points within the metallicity range of 8.6 to 9.4. This finding is consistent with the prediction of Timmes, Brown & Truran (2003) that the ^{56}Ni mass decreases by $0.15 M_{\odot}$ for the metallicity range in our sample (Equations 15-17; a blue curve in Figure 8c).

5.3. Environmental effects on supernova cosmology

We derive standardization parameters for maximum luminosity (α , β and M) and the Hubble residuals, a linear combination of them with lightcurve parameters (x_1 and c_{salt}) for these samples: EW H α , SFR SD, and metallicity. Luminosity standardization parameters are derived by minimizing χ^2 with the Hubble constant and cosmological parameters fixed. For this analysis, red SNe Ia with $c_{salt} > 0.3$ are treated the same as the rest. The datasets for EW H α , SFR SD, and metallicity consist of 81, 83, and 72 SNe Ia.

Table 2 summarizes the best fit luminosity standardization parameters and the HR root mean square(rms)s for these datasets. Hubble residuals are derived using these parameters. Several Hubble residuals of a SN Ia are derived if the SN Ia is contained in more than one sample. Their dependences on host gas properties are shown in Figure 9 for the samples of (a) EW H α , (b) SFR SD, and (c) metallicity. Five averaged Hubble residuals in each panel of Figures 9a and 9b are consistent with zero ($\sim 1\sigma$). We do not observe the average maximum brightness corrected for lightcurve shapes and colors to depend on EW H α and SFR SD. The Hubble residuals in the two lowest metallicity bins are 0.13 mag fainter than those in the three highest metallicity bins (1.8σ significance). Even though the significance is marginal, this corresponds to up to 6 % uncertainty in luminosity distance.

Further, we split each sample by their host characteristics and derived luminosity standardization parameters. Results are again summarized in Table 2. Figure 10 shows the significance levels in the differences of correction coefficients α (rectangles), β (circles) and M (triangles) between low/high EW H α , SFR SD and metallicity. Left (right) side points of each entry are the values for the sample with (without) the color cut. A significance is defined as the difference of a coefficient for low/high host properties divided by the root of an error sum of squares. Because of the many tests performed (Table 2), the significances on these results are less than what would be naively computed from the number of standard deviations. (i) SNe Ia in hosts with low EW H α have a marginally larger α , a marginally smaller β (1.7σ), and larger negative M (3.6σ) than those in hosts with high EW H α . (ii) SNe Ia in hosts with low SFR SD have a marginally larger α (1.6σ), a comparable β , and a

marginally smaller negative M than those in hosts with high SFR SD. (iii) SNe Ia in metal-poor hosts ($\log_{10}(\text{O}/\text{H})+12 < 9.0$) have a comparable α ($< 1\sigma$) to those in metal-rich hosts but have larger β (3.5σ) and marginally smaller negative M (1.8σ) than those in metal-rich hosts. (iv) $R_V \sim \beta - 1$ is smaller for SN Ia hosts, compared with the canonical value of $R_V = 3.1$ for our Galaxy. (v) The HR rms for SNe Ia in high EW $\text{H}\alpha$, high SFR SD and metal-rich hosts were smaller. These HR rms were comparable to 0.178 mag for the SDSS-II only sample (Kessler et al. 2009). When these parameters were calculated for the sample without red SNe Ia ($c_{\text{salt}} < 0.3$), the difference in β disappears below the 1σ level, while other parameters are barely changed.

6. Discussion

The relations between lightcurve characteristics of SNe Ia and their host gas properties have been investigated. EW $\text{H}\alpha$, SFR SD and metallicity has been used as host gas properties. For dependences of host galaxies on SN Ia properties, the averaged lightcurve width was narrower for SNe Ia occurring in hosts with lower EW $\text{H}\alpha$. This suggests that hosts with a lower EW $\text{H}\alpha$ give birth to SNe Ia with narrower widths of lightcurves. The lightcurve width was also narrower for SNe Ia in lower star forming rate hosts. Moreover, the ^{56}Ni mass was observed to have the best sensitivity to the EW $\text{H}\alpha$ of their hosts. Although this mass shows a wide scatter from ~ 0.2 to $1.0 M_{\odot}$, the average trend between the ^{56}Ni mass and metallicity was consistent with a theoretical prediction based on the nucleosynthesis (Timmes, Brown & Truran 2003). For the standardization of maximum luminosity, the HR averages were constant with respect to EW $\text{H}\alpha$ and SFR SD, indicating that the dependences of maximum luminosity on them were removed by lightcurve corrections. The coefficient β was large for SNe Ia in hosts with large EW $\text{H}\alpha$ and low metallicity.

Effects of host galaxies on SN Ia properties: Dependences of SN Ia lightcurve properties on host characteristics can be compared with a similar study using nearby SNe Ia and their hosts (Gallagher et al. 2005). Observing entire spectra of nearby galaxies, they measured emission line fluxes and derived EW $\text{H}\alpha$, SFR by the $\text{H}\alpha$ emission, and metallicity by the ratios of strong lines. Their result shows that the deviation of Δm_{15} for SNe Ia in hosts with low EW $\text{H}\alpha$ ($< 18 \text{ \AA}$) is more than twice larger than that for SNe Ia in hosts with high EW $\text{H}\alpha$. The differences between our findings and theirs probably results from sample selections. Around 80 % of SN Ia hosts in their sample are very bright nearby galaxies categorized before 1980 in the New General Catalogue, the Index Catalogue or the Uppsala General Catalogue of Galaxies.

Recently the ^{56}Ni mass was correlated with host metallicity (Howell et al. 2009; Neill

et al. 2009) derived from stellar masses and empirical calibrations (Tremonti et al. 2004; Liang et al. 2006). Howell et al. (2009) used over 100 pairs of SNe Ia and their host photometry in the high- z universe ($z \sim 0.4$) to report that the average of the ^{56}Ni mass becomes smaller for metal-rich hosts. Neill et al. (2009) used a similar size of SNe Ia and hosts in the local universe (regression velocity of $cz \lesssim 30,000\text{km sec}^{-1}$) and reported that although the data were statistically consistent with no trend, they were also consistent with the Howell et al. (2009) and the Timmes, Brown & Truran (2003) model. Their method of metallicity estimation is different from ours, since emission lines are formed by interstellar gases while photometry is primarily contributed by the stellar component. It can be said that our study has revealed the dependence of the ^{56}Ni mass on host *gas* metallicity.

Luminosity standardization: Gallagher et al. (2005) found insignificant correlations between HR and $\text{H}\alpha$ -emission related properties of the $\text{H}\alpha$ EW and the SFR SD, while they showed a slight trend of a negative HR for SNe Ia in metal-rich hosts. However, they cautioned that the trend was less than a 2σ detection. Our findings are consistent with theirs. We do not make comparisons with Gallagher et al. (2008), which ruled out a no-correlation at the 98 % significance level, because they analyzed different type hosts (passive) by a different metallicity estimation method (absorption lines).

Recent studies (Sullivan et al. 2010; Kelly et al. 2010; Lampeitl et al. 2010b) reported evidence at between 2 and 3σ that SNe Ia are brighter in massive hosts with low star formation per stellar mass (specific SFR), after their SN Ia maximum brightnesses have been standardized by using their lightcurve shapes and colors. If massive hosts are metal-rich, their results agree with brighter SNe Ia in metal-rich hosts after lightcurve corrections (Figure 9c).

We found a hint that SNe Ia have smaller ^{56}Ni mass on average in metal-rich hosts (Figure 8c). On the other hand, we found a marginally larger negative M (Table 2) and HR (Figure 9c) for such SNe Ia. Since the ^{56}Ni mass is the main source of the SN luminosity (Arnett 1982), smaller ^{56}Ni masses would result in a smaller negative M . There is also evidence of smaller negative M for SNe Ia in hosts with a high EW $\text{H}\alpha$ (Table 2). These findings agree with a former study (Sullivan et al. 2010) that SNe Ia in massive hosts becomes 0.08 mag ($\approx 4.0\sigma$) brighter after lightcurve corrections if massive hosts are metal-rich and have a low $\text{H}\alpha$. Kasen, Röpke & Woosley (2009) claimed from simulations that metal-rich progenitors cause SNe Ia both to be fainter and to have narrower lightcurves. They also showed that SNe Ia in metal-rich progenitors are brighter for a fixed decline rate of luminosity. Thus, our findings are qualitatively consistent with these studies.

There is evidence that β is larger for SNe Ia in metal-poor hosts or hosts with a large EW $\text{H}\alpha$. This suggests that the size of the color correction βc_{salt} is larger for SNe Ia with the

same color in hosts with metal-poor/large EW H α than those with metal-rich/low EW H α (Table 2). Similar results have been shown in Lampeitl et al. (2010b) that β is larger for SNe Ia in star forming hosts than passive hosts. An uncertainty of 0.16 in the β estimation for our 36 metal-poor galaxies is comparable to that of 0.16 for their 40 passive hosts. Sullivan et al. (2010) derived SFR and stellar mass to present a larger β for SNe Ia in the hosts with higher specific SFR and with lower stellar mass. If these galaxies are metal-poor and show large H α EWs, our results agree with theirs. Since metal-poor and star forming galaxies are dustier than metal-rich and passive galaxies, these findings might imply that large dust extinctions in hosts increase β .

As can be seen in Table 2, there might be evidence for a different α between low and high SFR SD hosts at between 1 and 2σ . If the effective α does depend on star formation rate, one would expect it also to be a function of redshift due to the increase in cosmic star formation with redshift (Lilly et al. 1996; Madau et al. 1998; Cowie et al. 1999; Flores et al. 1999; Haarsma et al. 2000; Wilson et al. 2002; Hopkins 2004; Hopkins & Beacom 2006) would introduce a change in α .

Progenitor model: It is well documented that CO WDs in a binary system can increase their masses by accretion from their companion star (e.g. Whelan & Iben 1973; Iben & Tuckey 1984). When their masses reach the Chandrasekhar limit, they are expected to explode as SNe Ia. An explosion model by Hachisu, Kato & Nomoto (1996) proposed that WDs below a metallicity cutoff can not explode as SNe Ia because they cannot produce a wind. Based on this scenario, Kobayashi et al. (1998) predicted a metallicity cutoff of $[\text{Fe}/\text{H}] = -1.1$. This value corresponds to $\log_{10}(\text{O}/\text{H})+12 = 8.0$ by Equation 17 and to $\log_{10}([\text{N II}]\lambda 6585/\text{H}\alpha) = -1.65$ by the calibration formula of Pettini & Pagel (2004). As shown in Figure 3, there are no SN Ia hosts below the metallicity of 8.0. Since the MPA/JHA database itself has a very low fraction ($< 0.1\%$) of such galaxies (Figure 3), the absence of SN Ia hosts might not be meaningful, but, they might support the Hachisu model.

Metal-poor hosts below the metallicity cutoff were obtained in the high-z samples of Howell et al. (2009) and Sullivan et al. (2010). However, the average metallicity drops by at most 0.1 dex (Rodrigues et al. 2008) between nearby and their largest redshift hosts. Thus, it is hard to believe that the existence of metal-poor hosts does not result from the usage of nearby empirical relations between stellar masses and metallicities (Tremonti et al. 2004; Liang et al. 2006). These hosts might imply a different channel to the SN Ia explosion from the Hachisu model. Spectroscopic observations of those galaxies will be of great help to discuss their metallicity effects.

7. Conclusions

We have analyzed the multi-band lightcurves of 118 confirmed SNe Ia and the spectra of their host galaxies. We derived the EW H α , SFR SD, and gas-phase metallicity from the spectra and compared these with the lightcurve widths and colors of SNe Ia. In addition, we compared host properties with the Hubble residuals corrected for lightcurve parameters to investigate uncorrected systematic effects in the magnitude standardization. We conclude the following:

(i) SNe Ia in hosts with a higher star formation rate, on average, have synthesized larger ^{56}Ni mass and show wider lightcurves. The ^{56}Ni mass dependence is consistent with a nucleosynthesis-based prediction.

(ii) SNe Ia in metal-rich galaxies ($\log_{10}(\text{O}/\text{H})+12 > 9.0$) have become 0.13 magnitude brighter (at the 1.8σ level) after lightcurve corrections, which corresponds to up to 6 % uncertainty in the luminosity distance.

(iii) The coefficient of the color correction term in standardizing luminosity is larger for SNe Ia in metal-poor hosts or hosts with a large EW H α (at the $\sim 2\sigma$ level).

Acknowledgements – K.K. thanks the COE Program “the Quantum Extreme Systems and Their Symmetries” for fiscal 2007, the Global COE Program “the Physical Sciences Frontier” for fiscal 2008-2010, MEXT, Japan and the JASSO scholarship for fiscal 2007-2009.

Funding for the SDSS and SDSS-II was provided by the Alfred P. Sloan Foundation, the Participating Institutions, the National Science Foundation, the U.S. Department of Energy, the National Aeronautics and Space Administration, the Japanese Monbukagakusho, the Max Planck Society, and the Higher Education Funding Council for England. The SDSS Web site is <http://www.sdss.org/>.

The SDSS is managed by the Astrophysical Research Consortium (ARC) for the Participating Institutions. The Participating Institutions are The University of Chicago, Fermilab, the Institute for Advanced Study, the Japan Participation Group, The Johns Hopkins University, Los Alamos National Laboratory, the Max-Planck-Institute for Astronomy (MPIA), the Max-Planck-Institute for Astrophysics (MPA), New Mexico State University, University of Pittsburgh, Princeton University, the United States Naval Observatory, and the University of Washington. This research has made use of the NASA/IPAC Extragalactic Database (NED) which is operated by the Jet Propulsion Laboratory, California Institute of Technology, under contract with the National Aeronautics and Space Administration.

Facilities: SDSS

REFERENCES

- Abazajian, K., et al., ApJS, 182, 543
- Aldering, G., Knop, R., & Nugent, P., AJ, 119, 2110
- Arnett, W.D. , 1982, ApJ, 253, 785
- Asplund, M., Grevesse, N., & Sauval, A.J. 2005 ASP Coference Series, Vol. 336, 2005
- Aubourg, E., Tojeiro, R., Jemenez, R., Heavens, A., Strauss, M.A., & Spergel, D.A. A&A, 492, 631
- Badenes, Carles, Bravo, Eduardo & Hughes, John P. 2008, ApJ, 680, 33
- Bartunov, O.S., Tsvetkov, D.Y., & Pavlyuk, N.N., 2007, Highlights Astron., 14, 316
- Boissier, S., & Prantzos, N., A&A, 503, 137
- Branch, D. & Khoklov, A.M. 1995, Phys. Rep., 256, 53
- Brandt, T.D., et al. 2010, AJ, 140, 804
- Calzetti, D., Kinney, A.L., & Storchi-Bergmann, T, 1994, ApJ, 429, 582
- Chamulak, D.A., Brown, E.F., Timmes, F.X., & Dupczak, K.Y., 2008, ApJ, 677, 160
- Charlot, S., & Longhetti, M. 2001, MNRAS, 323, 887
- Colgate, S.A. & Mckee, C. 1969, ApJ, 157, 623
- Conley, A., eta l. 2006, AJ, 132, 1707
- Cowie, L. L., Songaila, A., & Barger, A. J. 1999, AJ, 118, 603
- Dopita, M.A., & Evans, I.N. 1986, ApJ, 307, 431
- Edmunds, M.G., & Pagel, B.E.J. 1984, MNRAS, 211, 507
- Flores, H., et al. 1999, ApJ, 517, 148
- Frieman, J.A., et al. 2008, AJ, 135, 338

- Fukugita, M., Ichikawa, T., Gunn, J. E., Doi, M., Shimasaku, K., & Schneider, D. P. 1996, *AJ*, 111, 1748
- Gallagher, J.S., Garnavich, P.M., Berlind, P., Challis, P., Jha, S., & Kirshner, R.P. 2005, *ApJ*, 634, 210
- Gallagher, J.S., Garnavich, P.M., Caldwell, N., Kirshner, R.P., Jha, S.W., Li, W., Ganeshalingam, M., & Filippenko, A.V. 2008, *ApJ*, 2008, 685
- Goldhaber, G., et al., 2001, *AJ*, 558, 359
- Gordon, K.D., et al., 2003, *ApJ*, 594, 279
- Gunn, J. E., et al. 1998, *AJ*, 116, 3040
- Gunn, J. E., et al. 2006, *AJ*, 131, 2332
- Guy, J., et al. 2005, *A&A*, 443, 781
- Guy, J., et al. 2007, *A&A*, 466, 11
- Guy, J., et al. 2010, arXiv:1010.4743v1
- Haarsma, D. B., Partridge, R. B., Windhorst, R. A., & Richards, E. A. 2000, *ApJ*, 544, 641
- Hachisu, I., Kato, M., & Nomoto, K., 1996, *ApJ*, 470, L97
- Hamuy, M., Trager, S.C., Pinto, P.A., Phillips, M.M., Schommer, R.A., Ivanov, V. & Suntzeff, N.B. 2000, *AJ*, 120, 1479
- Hayden, B.T., et al. 2010, *ApJ*, 712, 350
- Henry, R.B.C., & Worthey, G., 1999, *PASP*, 111, 919
- Hicken, M., 2009, *ApJ*, 700, 1097
- Hillebrandt, W. & Niemeyer, J.C. 2000, *ARA&A*, 38, 191
- Holtzman, J.A., et al. 2008, *AJ*, 136, 2306
- Hopkins, A. M. 2004, *ApJ*, 615, 209
- Hopkins, A.M. & Beacom, J.F., *ApJ*, 651, 142
- Howell, A., et al. 2006, *Nature*, 443, 308

- Howell, A., et al. 2009, *ApJ*, 691, 661
- Höflich, P., Wheeler, J.C., & Thielemann, F.K., 1998, *ApJ*, 495, 617
- Höflich, P., Nomoto, K., Umeda, H., & Wheeler, J.C., 2000, *ApJ*, 528, 590
- Hsiao, E. Y., Conley, A., Howell, D. A., Sullivan, M., Pritchett, C. J., Carlberg, R. G., Nugent, P. E., & Phillips, M. M. 2007, *ApJ*, 663, 1187
- Iben, I., & Tutukov, A.V. 1984, *ApJS*, 54, 335
- Jha, S., Riess, A.G., Kirshner, R.P., 2007, *ApJ*, 659, 122
- Kasen, D., & Woosley, S.E., 2007, *ApJ*, 656, 661
- Kasen, D., Röpke, F.K., & Woosley, S.E., *Nature*, 460, 869
- Kauffmann, G., et al., 2003, *MNRAS*, 346, 1055
- Kelly, P.L., et al. 2010, *ApJ*, 715, 743
- Kennicutt, R.C., Jr. 1998, *ApJ*, 498, 541
- Kessler, R., et al. 2009, *ApJS*, 185, 32.
- Kewley, L.J. & Dopita, M.A., 2002, *ApJS*, 142, 35
- Kewley, L.J., Ellison, S.L., 2008, *ApJ*, 681, 1183
- Kobayashi, C., Tsujimoto, T., Nomoto, K., Hachisu, I. & Kato, M. 1998, *ApJ*, 503, L155
- Kobulnicky, H.A., Kennicutt, R.C., & Pizagno, J.L. 1999, *ApJ*, 514, 544
- Kobulnicky, H.A., & Kewley, L.J. *ApJ*, 617, 240
- Kowalski, M., et al. 2008, *ApJ*, 686, 749
- Lampeitl, H., et al., 2010, *MNRAS*, 401, 2331
- Lampeitl, H., et al., 2010, arXiv 1005.4687
- Lentz, E. J., Baron, E., Branch, D., Hauschildt, P. H., & Nugent, P. E. 2000, *ApJ*, 530, 966
- Liang, Y. C., Yin, S. Y., Hammer, F., Deng, L. C., Flores, H., Zhang, B., 2006, *ApJ*, 652, 257L
- Lilly, S. J., Le Fevre, O., Hammer, F., & Crampton, D. 1996, *ApJ*, 460, L1

- Madau, P., della Valle, M., & Panagia, N. 1998, MNRAS, 297, L17
- McCall, M.L., Rybski, P.M., & Shields, G.A. 1985, ApJS, 57, 1
- McClelland, C.M., et al. arXiv:1007.2850
- McGaugh, S.S. 1991, ApJ, 380, 140
- Neill, J.D., et al., 2009, ApJ, 707, 1449
- Nobili, S. & Goobar, A. 2008, A&A, 487, 19
- Osterbrock, D.E. 1989, Astrophysics of gaseous nebulae and active galactic nuclei, Research supported by the University of California, John Simon Guggenheim Memorial Foundation, University of Minnesota (Mill Valley CA: University Science Books), 422
- Nordin, J., et al., 2010, arXiv: 1012.4430
- Pagel, B.E.J., & Edmunds, M.G., 1981, ARA&A, 19, 77
- Perlmutter, S., et al., 1997, ApJ, 483, 565
- Perlmutter, S. et al., 1999, ApJ, 517, 565
- Pettini, M. & Pagel, B.E.J. 2004, MNRAS, 348, L59
- Phillips, M.M. 1993, ApJ, 413, L105
- Phillips, M.M., Lira, P., Suntzeff, N.B., Schommer, R.A., Hamuy, M. & Maza, J. 1999, AJ, 118, 1766
- Phillips, M.M., et al., 2007, PASP, 119, 360
- Ramirez, I., Prieto, A., & Lambert, D.L. 2007, A&A, 465, 271
- Riess, A.G., Press, W.H. & Kirshner, R.P. 1996, ApJ, 473, 88
- Riess, A. G., et al. 1998, AJ, 116, 1009
- Riess, A. G., et al. 1999, AJ, 117, 707
- Rodrigues, M., et al. 2008, A&A, 492, 371
- Röpke, F.K., Gieseler, M., Reinecke, M., Travaglio, C., & Hillebrandt, W. 2006, A&A, 453, 203

- Sako, M., et al. 2008, AJ, 135, 348
- Sauer, D.N., et al. 2008, MNRAS, 391, 1605
- Stoughton, C., et al., 2002, AJ, 123, 485
- Stritzinger, M., et al., 2006, A&A, 460, 793
- Sullivan, M., et al., 2010, MNRAS, 406, 782
- Takanashi, N., Doi, M. & Yasuda, N. 2008, MNRAS, 389, 1577
- Timmes, F.X., Brown, E.F. & Truran, J.W. 2003, ApJ, 590, L83
- Travaglio, C., Hillebrandt, W., & Reinecke, M. 2005, A&A, 443, 1007
- Tremonti, C.A., et al., 2004, MNRAS, 613, 898
- Tripp, R., 1998, A&A, 331, 815
- Truran, J.W., Arnett, W.D. & Cameron, A.G.W. Canadian Journal of Physics, 45, 2315
- Veilleux, S., & Osterbrock, D.E., 1987, ApJS, 63, 295
- Vila-Costas, M.B., & Edmunds, M.G., 1993, MNRAS, 265, 199
- X. Wang, et al., 2009, ApJ, 697, 380
- Wheeler, J.C., Sneden, C., & Truran, Jr., 1989, ARA&A, 27, 279
- Whelan, J., & Iben, I., 1973, ApJ, 186, 1007
- Wilson, G., Cowie, L. L., Barger, A., & Burke, D. J. 2002, AJ, 124, 1258
- Yasuda, N. & Fukugita, M., AJ, 139, 39
- York, D.G., et al. 2000, AJ, 120, 1579
- Zaritsky, D., Kennicutt, R.C. & Huchra, J.P. 1994, ApJ, 420, 87

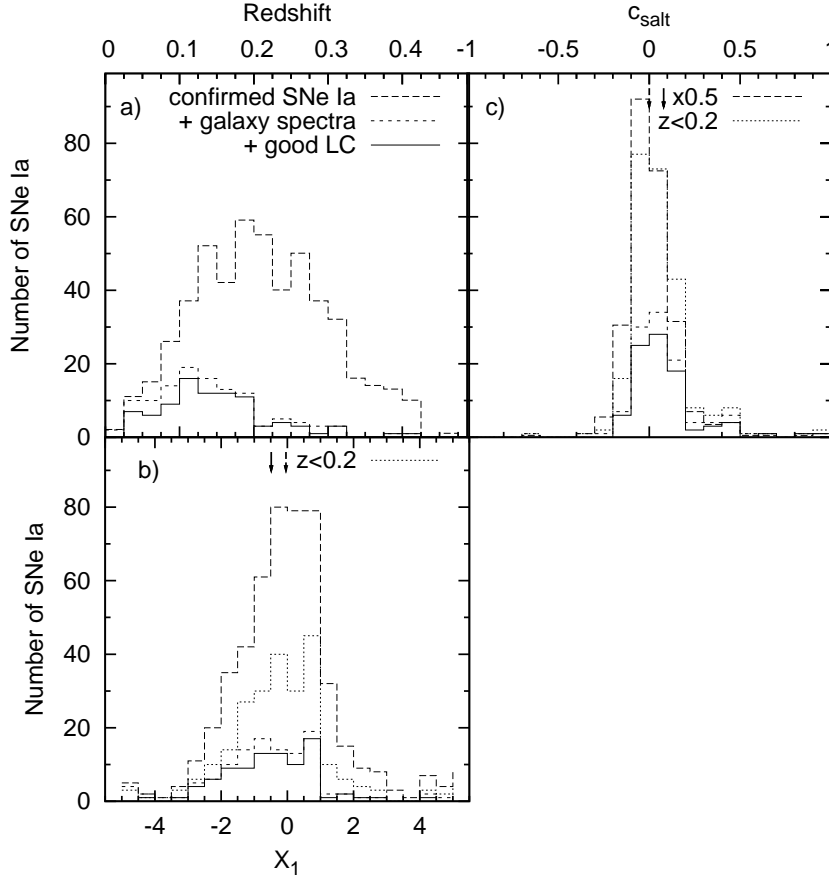


Fig. 1.—: Distributions of (a) redshift, (b) lightcurve width x_1 , and (c) color c_{salt} distributions for 512 spectroscopically confirmed SNe Ia (bold dashed line), 118 of them with SDSS galaxy spectra (thin dashed lines), and 86 of them that pass all the lightcurve criteria (solid lines; good LC). The arrows in the x_1 and c_{salt} distributions are the averages of confirmed SNe Ia and the good LC sample. The average lightcurve parameters for the good LC sample show a lower x_1 and a higher c_{salt} relative to the confirmed SNe Ia. The color histogram for 512 confirmed SNe Ia is multiplied by 0.5 for illustrative purposes. Dotted histograms for x_1 and c_{salt} distributions are confirmed SNe Ia at $z < 0.2$. The x_1 distributions for SNe Ia at $z < 0.2$ and the good LC sample come from the same distribution with a 68% probability and the c_{salt} distribution with a 98 % probability.

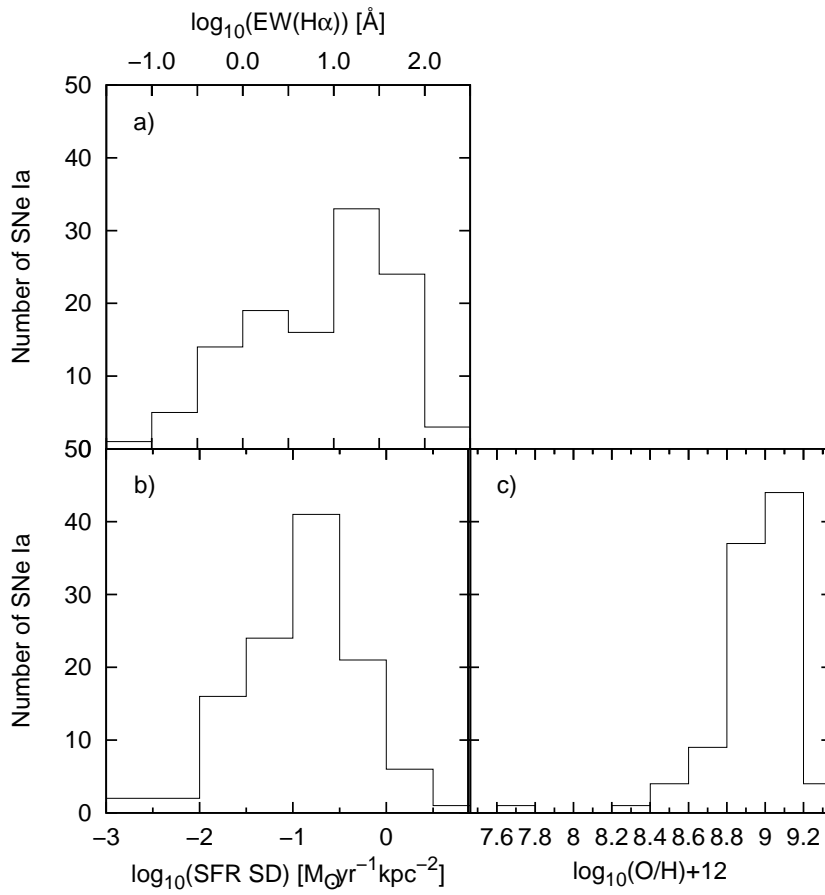


Fig. 2.—: Distributions of (a) EW H α , (b) SFR surface density (SFR SD), and (c) metallicity for host galaxies from our measurements.

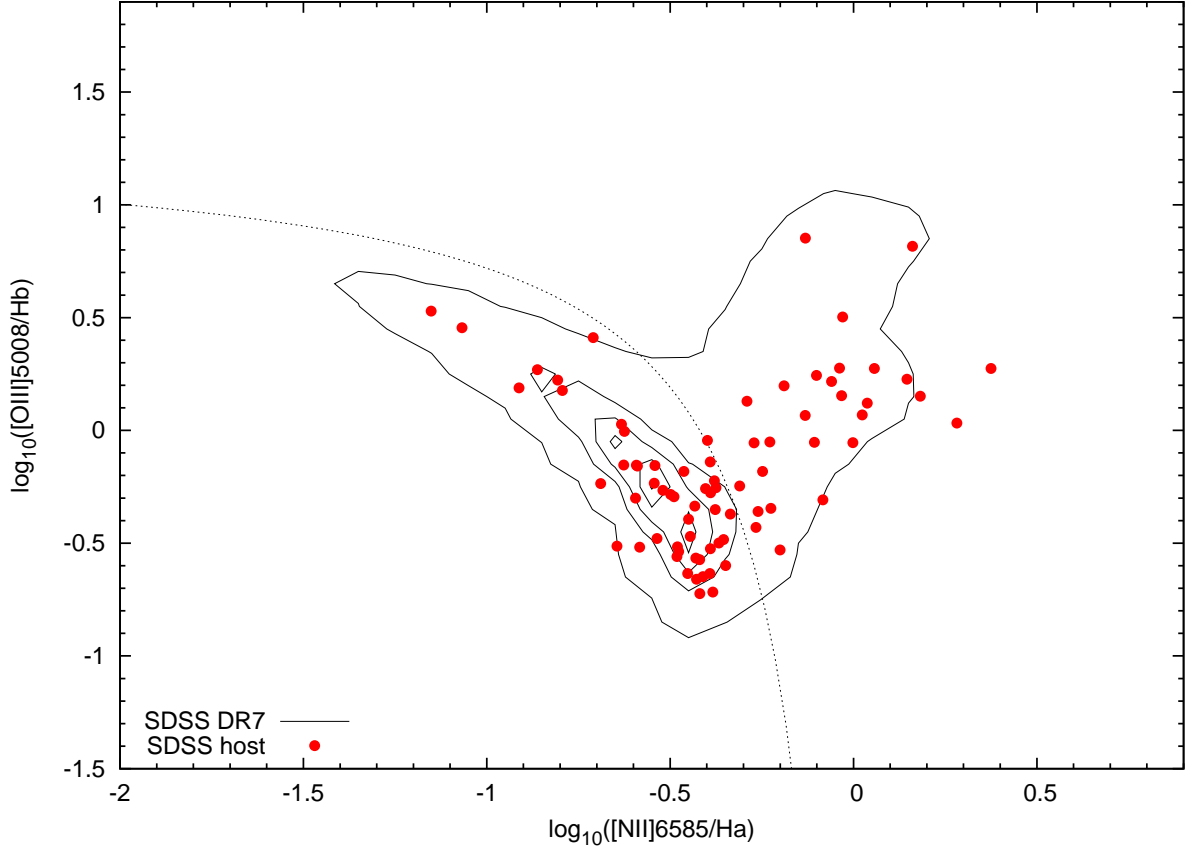


Fig. 3.—: $[\text{N II}]\lambda 6585/\text{H}\alpha$ vs. $[\text{O III}]\lambda 5008/\text{H}\beta$ flux ratios. The distributions of over 170,000 galaxies for the MPA/JHA sample are shown as the black contour lines (100, 2500, 5000, 7500, 10000 galaxies from outer to inner), whereas SN Ia host galaxies are in red. The black curve shows the demarcation between star forming galaxies (left bottom) and AGN-like galaxies (right top) from Kauffmann et al. (2003).

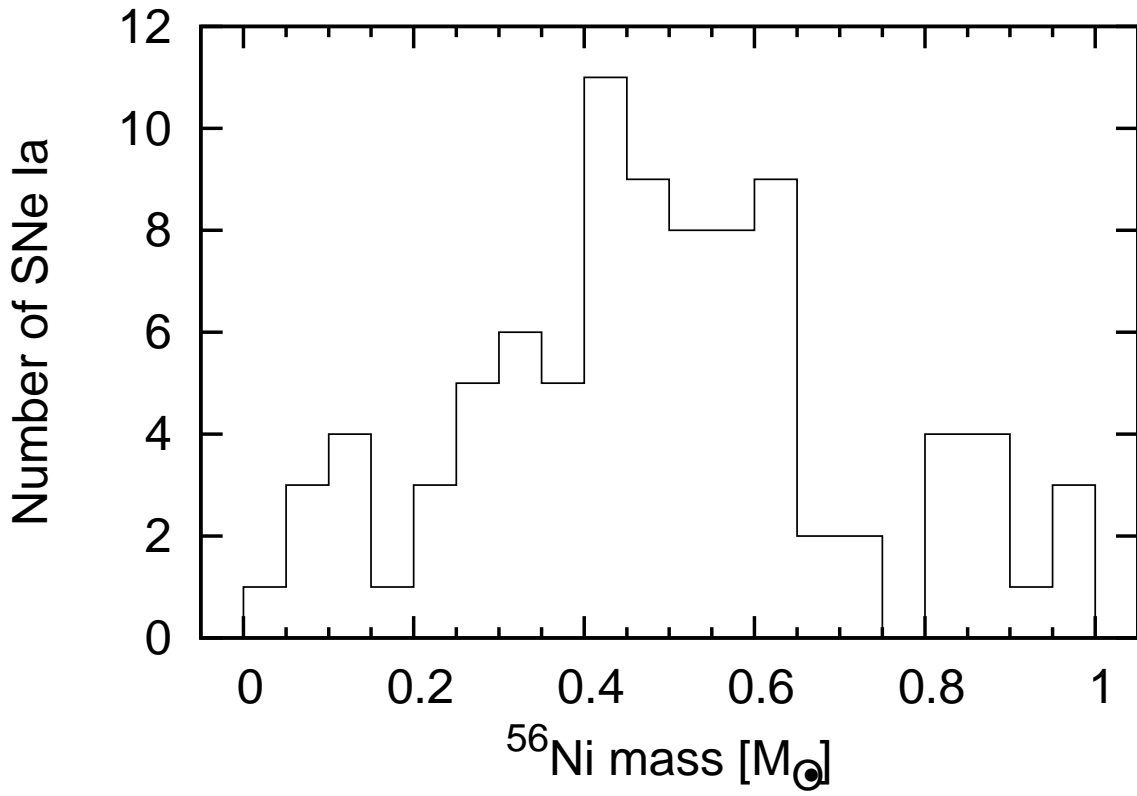


Fig. 4.—: The distribution of ^{56}Ni masses for our sample for the good LC sample.

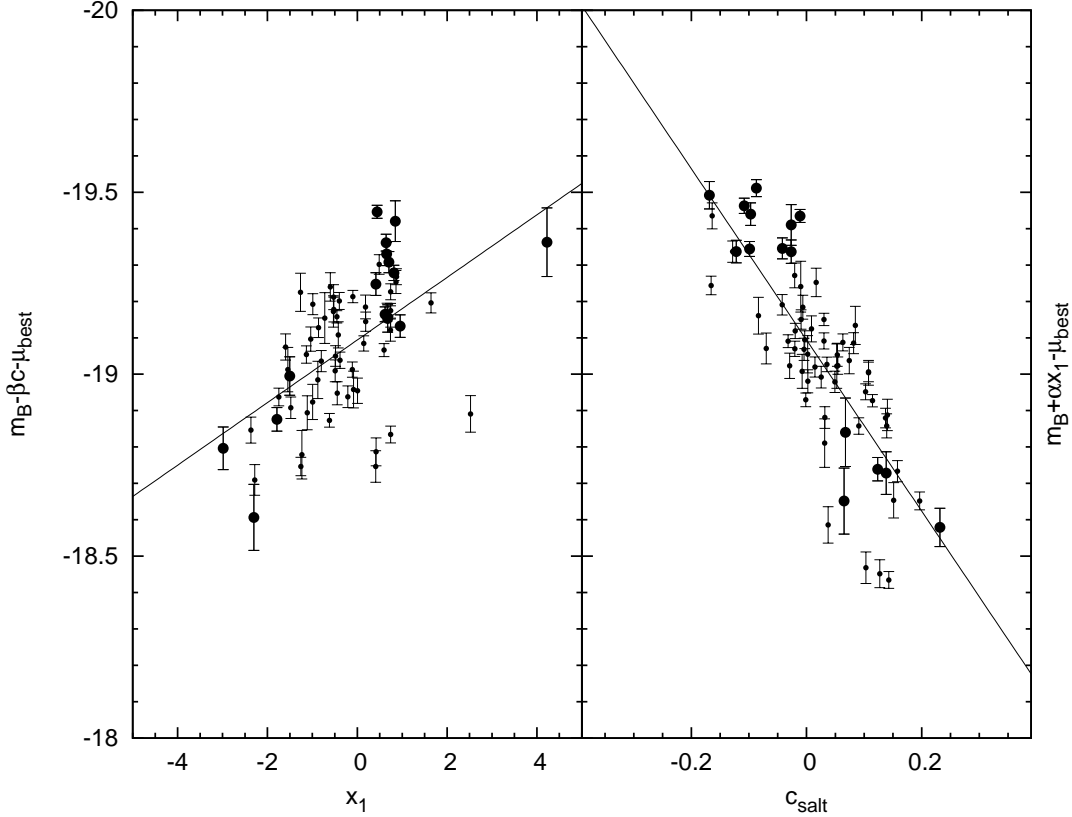


Fig. 5.— The magnitude-width and magnitude-color relations. Left: the color-corrected magnitude $m_B - \beta c - \mu_{best}$ is plotted against the width x_1 . Right: the width-corrected magnitude $m_B + \alpha x_1 - \mu_{best}$ is plotted against the color c_{salt} . SNe Ia with the ^{56}Ni mass $< 0.3 M_\odot$ or $> 0.8 M_\odot$ are marked with circles, while the others with dots. The lines in the figures have the values of α , β and M which minimize $\chi^2 = \sum \left(\frac{HR^2}{(\delta\mu_B)^2 + \sigma_{int}^2} \right)$.

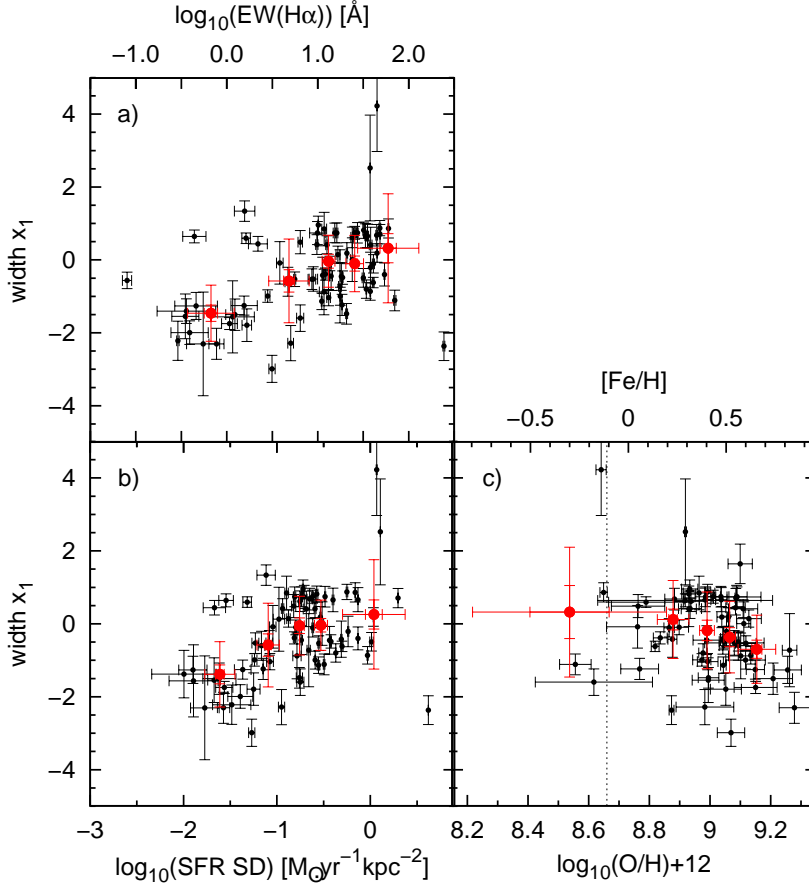


Fig. 6.—: The dependences of the SN Ia lightcurve width x_1 on host gas properties: (a) H α EW, (b) SFR SD, and (c) metallicity. The metallicity is represented as $\log_{10}(\text{O}/\text{H})+12$ (lower scale) or $[\text{Fe}/\text{H}]$ (upper scale). Note that $[\text{Fe}/\text{H}]$ is negative for thin disk stars with $[\text{O}/\text{H}]=0$. The vertical dotted line indicates the value of solar metallicity. Our sample is plotted as black dots. The red points are the mean widths, the error on the mean, and the deviation for each set of 15 SNe Ia from the highest value of host EW H α , SFR SD, and metallicity. One SNe Ia with the lowest metallicity host of $\log_{10}(\text{O}/\text{H})+12 < 8.2$ is eliminated from the figure for illustrative purposes.

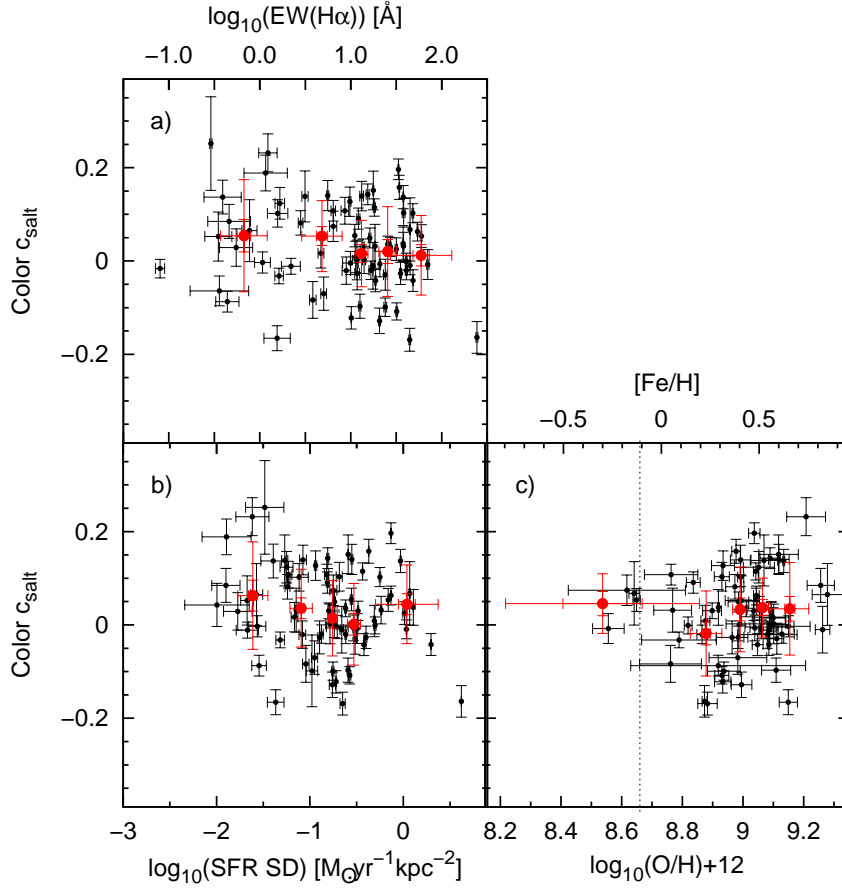


Fig. 7.—: The dependences of the SN Ia color c_{salt} on host gas properties: (a) H α EW, (b) SFR SD and (c) metallicity. The symbols are the same as Figure 6.

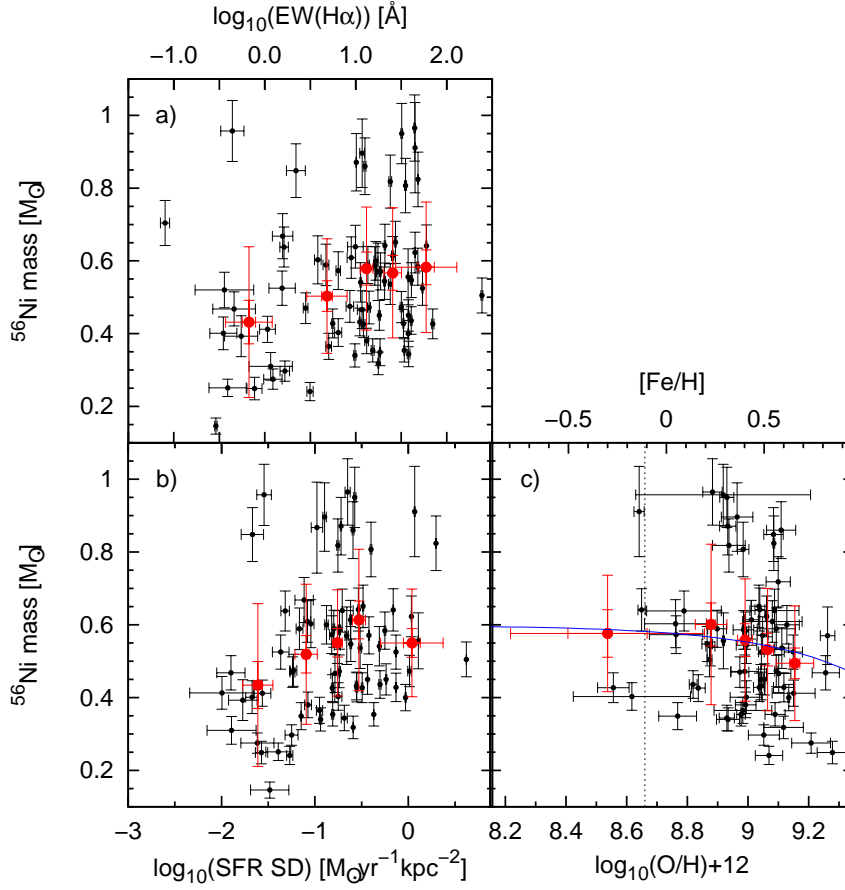


Fig. 8.—: The dependences of the ^{56}Ni mass on host gas properties: (a) EW $\text{H}\alpha$, (b) SFR SD and (c) metallicity. The symbols are the same as Figure 6. The blue curve is the theoretical prediction of Timmes, Brown & Truran (2003).

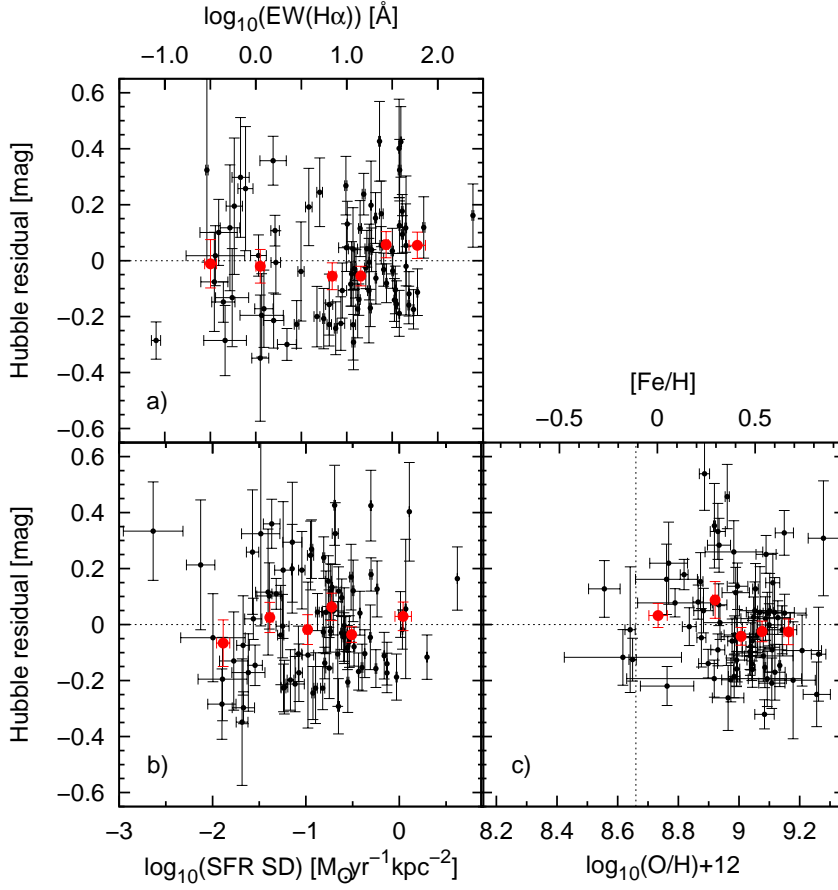


Fig. 9.—: The dependences of the Hubble residuals on host gas properties: (a) $\text{H}\alpha$ EW, (b) SFR SD and (c) metallicity. The symbols are the same as Figure 6. Five averaged Hubble residuals in each panel of (a) and (b) are consistent with zero ($\sim 1\sigma$). The Hubble residuals in the two lowest metallicity bins are 0.13 mag fainter than those in the three highest metallicity bins ($\sim 1.8\sigma$ significance; panel c).

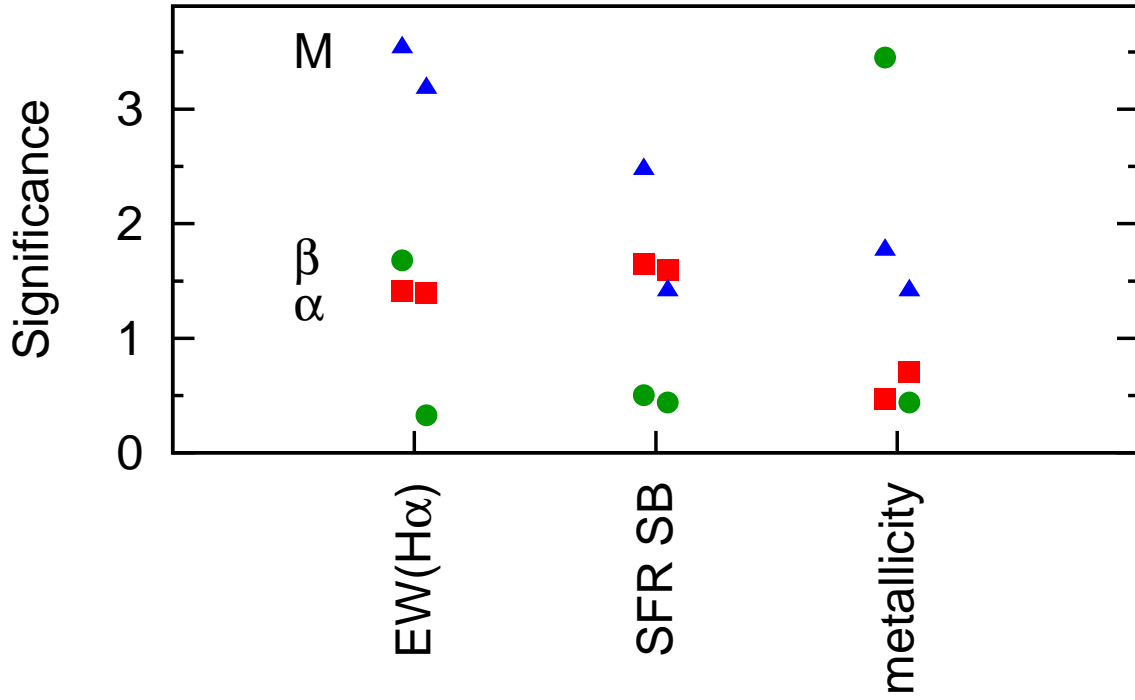


Fig. 10.—: Significance levels in the differences of correction coefficients α (rectangles), β (circles) and M (triangles) between low/high EW H α , SFR SD and metallicity. Left (right) side points of each entry are the values for the sample with (without) the color cut.

Table 1. Summary of spectroscopic properties of the SDSS host galaxy

ID ^a	IAU name	EW (H α)	$E(B - V)$	SFR [$M_{\odot} \text{ yr}^{-1} \text{ kpc}^{-2}$]	$\log_{10}(\text{O}/\text{H})+12$	Calib ^b	Env ^c
722	2005ed	1.99 ± 0.17	-0.00 ± 0.26	$(9.53 \pm 1.04) \times 10^{-2}$	9.045 ± 0.042	N2/O2a	AGN
739	2005ef	1.58 ± 0.26	—	$(6.53 \pm 1.13) \times 10^{-2}$	9.200 ± 0.046	N2/O2g	N/A
762	2005eg	9.92 ± 2.12	0.49 ± 0.39	$(1.96 \pm 0.57) \times 10^{-1}$	9.087 ± 0.081	N2/O2a	AGN
774	2005ex	5.09 ± 0.26	1.28 ± 0.40	$(2.99 \pm 0.13) \times 10^{-1}$	8.658 ± 0.086	N2/O2a	AGN
1032	2005ez	3.14 ± 0.27	-0.23 ± 0.20	$(5.37 \pm 0.46) \times 10^{-2}$	9.069 ± 0.045	N2/O2a	AGN
1112	2005fg	11.71 ± 1.48	0.48 ± 0.29	$(1.64 \pm 0.18) \times 10^{-1}$	9.101 ± 0.040	N2/O2g	AGN
1371	2005fh	0.44 ± 0.14	-0.21 ± 0.23	$(2.85 \pm 0.56) \times 10^{-2}$	8.918 ± 0.288	N2/S2h	AGN
1580	2005fb	48.40 ± 0.33	0.54 ± 0.04	$(1.98 \pm 0.02) \times 10^0$	9.085 ± 0.003	N2/O2a	AGN
2561	2005fv	12.12 ± 0.53	0.75 ± 0.04	$(1.54 \pm 0.05) \times 10^{-1}$	8.836 ± 0.023	N2/O2a	SF
2689	2005fa	1.57 ± 0.44	—	$(7.65 \pm 1.88) \times 10^{-2}$	N/A	caseX	N/A
2992	2005gp	13.19 ± 0.66	0.49 ± 0.25	$(8.43 \pm 0.77) \times 10^{-2}$	8.992 ± 0.034	N2/O2a	SF
3592	2005gb	18.72 ± 0.30	0.64 ± 0.05	$(3.79 \pm 0.06) \times 10^{-1}$	9.048 ± 0.018	N2/O2a	AGN
3901	2005ho	59.82 ± 0.61	0.22 ± 0.02	$(6.89 \pm 0.06) \times 10^{-1}$	8.649 ± 0.012	N2/O2a	SF
5944	2005hc	1.63 ± 0.19	-0.16 ± 0.21	$(4.80 \pm 0.54) \times 10^{-2}$	8.789 ± 0.123	N2/S2h	AGN
5966	2005it	17.58 ± 0.69	0.18 ± 0.09	$(2.19 \pm 0.10) \times 10^{-1}$	9.262 ± 0.024	N2/O2a	SF
6057	2005if	34.25 ± 0.32	0.19 ± 0.03	$(4.26 \pm 0.02) \times 10^{-1}$	8.977 ± 0.014	N2/O2a	SF
6295	2005js	0.52 ± 0.14	—	$(3.93 \pm 1.32) \times 10^{-2}$	N/A	caseX	N/A
6406	2005ij	13.62 ± 0.48	0.49 ± 0.11	$(1.59 \pm 0.04) \times 10^{-1}$	8.898 ± 0.031	N2/O2a	SF
7876	2005ir	20.91 ± 0.39	0.32 ± 0.05	$(2.92 \pm 0.05) \times 10^{-1}$	9.039 ± 0.016	N2/O2a	SF
8151	2005hk	9.71 ± 0.33	0.06 ± 0.07	$(1.55 \pm 0.04) \times 10^{-1}$	8.229 ± 0.050	N2/S2h	N/A
10028	2005kt	0.35 ± 0.13	—	$(2.12 \pm 0.36) \times 10^{-2}$	8.994 ± 0.053	N2/O2g	N/A
10096	2005lj	22.92 ± 0.58	0.16 ± 0.05	$(2.03 \pm 0.04) \times 10^{-1}$	8.886 ± 0.017	N2/O2a	SF
10434	2005lk	3.83 ± 0.35	0.54 ± 0.24	$(9.04 \pm 0.78) \times 10^{-2}$	8.761 ± 0.102	N2/S2h	AGN
10805	2005ku	37.62 ± 0.04	0.32 ± 0.02	$(1.28 \pm 0.00) \times 10^0$	8.919 ± 0.003	N2/O2a	SF
12778	2006fs	20.26 ± 0.33	0.40 ± 0.06	$(4.79 \pm 0.08) \times 10^{-1}$	8.953 ± 0.018	N2/O2a	SF
12781	2006er	0.77 ± 0.16	-0.46 ± 0.15	$(2.68 \pm 0.44) \times 10^{-2}$	9.278 ± 0.050	N2/O2a	SF
12843	2006fa	0.46 ± 0.27	-0.67 ± 0.58	$(1.26 \pm 0.48) \times 10^{-2}$	9.256 ± 0.045	N2/O2d	SF
12856	2006fl	23.95 ± 0.95	0.18 ± 0.11	$(1.76 \pm 0.05) \times 10^{-1}$	8.937 ± 0.054	N2/O2a	SF
12874	2006fb	11.75 ± 0.78	0.63 ± 0.16	$(1.27 \pm 0.06) \times 10^{-1}$	8.964 ± 0.052	N2/O2g	N/A
12897	2006eb	1.18 ± 0.11	0.28 ± 0.20	$(1.03 \pm 0.07) \times 10^{-1}$	8.938 ± 0.161	N2/S2h	N/A
12950	2006fy	40.73 ± 1.04	0.05 ± 0.03	$(4.97 \pm 0.15) \times 10^{-1}$	8.819 ± 0.013	N2/O2a	SF
12971	2006ff	1.16 ± 0.18	—	$(3.65 \pm 0.44) \times 10^{-2}$	8.912 ± 0.236	N2/Hai	N/A
12979	2006gf	0.68 ± 0.16	—	$(7.14 \pm 1.82) \times 10^{-2}$	N/A	caseX	N/A
12983	2006gl	85.57 ± 2.18	0.57 ± 0.07	$(4.06 \pm 0.17) \times 10^{-1}$	8.978 ± 0.019	N2/O2a	SF
13070	2006fu	44.54 ± 1.09	0.48 ± 0.12	$(2.24 \pm 0.16) \times 10^{-1}$	8.883 ± 0.032	N2/O2a	SF
13072	2006fi	243.83 ± 6.44	0.19 ± 0.00	$(4.19 \pm 0.00) \times 10^0$	8.873 ± 0.008	N2/O2a	SF
13099	2006gb	23.97 ± 1.21	0.29 ± 0.08	$(3.05 \pm 0.12) \times 10^{-1}$	9.111 ± 0.023	N2/O2a	SF
13135	2006fz	1.07 ± 0.23	—	$(2.73 \pm 0.63) \times 10^{-2}$	9.150 ± 0.071	N2/O2g	N/A
13254	2006gx	38.16 ± 1.38	0.17 ± 0.11	$(2.06 \pm 0.17) \times 10^{-1}$	8.930 ± 0.025	N2/O2a	SF
13354	2006hr	48.18 ± 1.12	0.37 ± 0.04	$(5.62 \pm 0.11) \times 10^{-1}$	8.992 ± 0.010	N2/O2a	SF
13511	2006hh	5.04 ± 0.40	0.67 ± 0.35	$(1.12 \pm 0.09) \times 10^{-1}$	8.983 ± 0.095	N2/O2d	N/A
13610	2006hd	74.48 ± 1.12	0.36 ± 0.03	$(9.25 \pm 0.12) \times 10^{-1}$	8.906 ± 0.009	N2/O2a	SF
14279	2006hx	5.58 ± 0.16	0.55 ± 0.08	$(2.81 \pm 0.07) \times 10^{-1}$	9.118 ± 0.034	N2/O2a	AGN
14284	2006ib	0.08 ± 0.01	—	N/A	N/A	caseX	N/A
14318	2006py	3.81 ± 0.27	0.46 ± 0.23	$(6.76 \pm 0.39) \times 10^{-2}$	8.878 ± 0.038	N2/O2a	AGN
14421	2006ia	1.55 ± 0.56	0.09 ± 0.44	$(4.30 \pm 0.95) \times 10^{-2}$	9.149 ± 0.030	N2/O2d	SF

Table 1—Continued

ID ^a	IAU name	EW (H α)	$E(B - V)$	SFR [$M_{\odot} \text{ yr}^{-1} \text{ kpc}^{-2}$]	$\log_{10}(\text{O}/\text{H})+12$	Calib ^b	Env ^c
14816	2006ja	2.81 ± 0.18	0.49 ± 0.22	$(5.75 \pm 0.37) \times 10^{-2}$	8.973 ± 0.030	N2/O2a	AGN
15129	2006kq	20.75 ± 0.53	0.40 ± 0.13	$(1.74 \pm 0.14) \times 10^{-1}$	8.995 ± 0.034	N2/O2a	SF
15136	2006ju	37.77 ± 0.36	0.39 ± 0.03	$(9.34 \pm 0.16) \times 10^{-1}$	9.134 ± 0.003	N2/O2a	SF
15161	2006jw	8.93 ± 1.04	0.30 ± 0.22	$(8.30 \pm 0.75) \times 10^{-2}$	9.080 ± 0.098	N2/O2a	SF
15222	2006jz	6.41 ± 0.64	—	$(1.78 \pm 0.17) \times 10^{-1}$	8.617 ± 0.193	N2/S2h	N/A
15234	2006kd	15.35 ± 0.61	0.26 ± 0.10	$(1.55 \pm 0.05) \times 10^{-1}$	9.089 ± 0.033	N2/O2a	SF
15421	2006kw	40.93 ± 1.21	0.08 ± 0.05	$(2.42 \pm 0.05) \times 10^{-1}$	8.865 ± 0.017	N2/O2a	SF
15425	2006kx	2.20 ± 0.57	—	$(2.14 \pm 0.64) \times 10^{-2}$	9.084 ± 0.032	N2/O2g	N/A
15443	2006lb	32.02 ± 0.78	0.26 ± 0.07	$(2.67 \pm 0.08) \times 10^{-1}$	8.930 ± 0.023	N2/O2a	SF
15467	— ^d	35.30 ± 1.03	0.27 ± 0.08	$(3.99 \pm 0.10) \times 10^{-1}$	8.984 ± 0.019	N2/O2a	SF
15648	2006ni	1.23 ± 0.31	-0.53 ± 0.62	$(2.42 \pm 1.07) \times 10^{-2}$	9.208 ± 0.064	N2/O2g	N/A
15734	2006ng	44.91 ± 0.37	0.16 ± 0.02	$(1.17 \pm 0.02) \times 10^0$	8.641 ± 0.017	N2/O2a	SF
16069	2006nd	33.51 ± 0.48	0.61 ± 0.04	$(7.37 \pm 0.10) \times 10^{-1}$	9.037 ± 0.019	N2/O2a	SF
16099	2006nm	-1.85 ± 1.27	—	N/A	9.099 ± 0.040	N2/O2g	N/A
16211	2006nm	0.40 ± 1.08	—	$(8.03 \pm 94.20) \times 10^{-4}$	N/A	N/A	N/A
16215	2006ne	7.56 ± 0.29	0.36 ± 0.09	$(1.19 \pm 0.04) \times 10^{-1}$	9.142 ± 0.048	N2/O2a	SF
16259	2006ol	1.66 ± 0.22	0.03 ± 0.38	$(5.62 \pm 0.97) \times 10^{-2}$	9.052 ± 0.051	N2/O2a	SF
16280	2006hz	0.58 ± 0.13	—	$(5.69 \pm 1.29) \times 10^{-2}$	N/A	caseX	N/A
16314	2006oa	29.52 ± 1.50	0.24 ± 0.10	$(4.78 \pm 0.17) \times 10^{-2}$	8.730 ± 0.060	N2/O2a	SF
16333	2006on	0.28 ± 0.19	-0.20 ± 0.31	$(2.60 \pm 0.28) \times 10^{-2}$	9.124 ± 0.041	N2/O2a	SF
16392	2006ob	1.04 ± 0.12	0.20 ± 0.30	$(1.60 \pm 0.19) \times 10^{-1}$	9.092 ± 0.058	N2/O2a	AGN
16482	2006pm	0.55 ± 0.25	—	$(1.69 \pm 0.65) \times 10^{-2}$	N/A	caseX	N/A
16644	2006pt	19.69 ± 2.14	0.53 ± 0.05	$(2.36 \pm 0.02) \times 10^{-1}$	9.036 ± 0.021	N2/O2a	SF
16692	2006op	5.23 ± 0.35	0.39 ± 0.20	$(5.36 \pm 0.24) \times 10^{-2}$	8.873 ± 0.065	N2/O2a	N/A
16789	2006pz	0.37 ± 0.40	—	$(8.42 \pm 21.00) \times 10^{-3}$	N/A	N/A	N/A
17117	2006qm	104.18 ± 1.25	0.20 ± 0.01	$(1.19 \pm 0.01) \times 10^0$	8.881 ± 0.007	N2/O2a	SF
17134	— ^d	15.33 ± 0.49	0.42 ± 0.04	$(0.00 \pm 0.00) \times 10^0$	8.987 ± 0.018	N2/O2a	SF
17135	2006rz	27.24 ± 0.43	0.04 ± 0.01	$(0.00 \pm 0.00) \times 10^0$	8.563 ± 0.020	N2/O2a	N/A
17171	2007id	0.52 ± 0.38	—	$(1.68 \pm 0.57) \times 10^{-2}$	N/A	N2/Hai	N/A
17176	2007ie	49.41 ± 0.11	0.11 ± 0.04	$(2.33 \pm 0.01) \times 10^{-1}$	8.438 ± 0.046	N2/O2a	SF
17186	2007hx	9.77 ± 0.32	0.58 ± 0.14	$(1.15 \pm 0.04) \times 10^{-1}$	8.934 ± 0.038	N2/O2a	AGN
17215	2007hy	1.38 ± 0.01	—	$(2.51 \pm 0.73) \times 10^{-2}$	9.091 ± 0.038	N2/O2g	N/A
17280	2007ia	20.88 ± 0.26	0.39 ± 0.02	$(6.10 \pm 0.02) \times 10^{-1}$	9.122 ± 0.029	N2/O2a	AGN
17332	2007jk	8.63 ± 0.91	0.36 ± 0.29	$(5.87 \pm 0.54) \times 10^{-2}$	7.773 ± 0.321	N2/S2h	AGN
17340	2007kl	4.71 ± 0.38	—	$(6.83 \pm 0.62) \times 10^{-2}$	9.093 ± 0.063	N2/O2g	N/A
17366	2007hz	12.61 ± 0.38	0.37 ± 0.09	$(2.56 \pm 0.07) \times 10^{-1}$	9.109 ± 0.048	N2/O2g	N/A
17497	2007jt	25.44 ± 0.80	0.40 ± 0.08	$(2.41 \pm 0.06) \times 10^{-1}$	9.011 ± 0.023	N2/O2g	SF
17500	2007lf	1.87 ± 0.12	-0.20 ± 0.12	$(2.15 \pm 0.15) \times 10^{-1}$	9.130 ± 0.018	N2/O2a	AGN
17784	2007jg	18.48 ± 0.08	0.17 ± 0.06	$(7.11 \pm 0.02) \times 10^{-2}$	8.768 ± 0.062	N2/O2a	N/A
17880	2007jd	17.69 ± 0.25	0.27 ± 0.06	$(2.57 \pm 0.02) \times 10^{-1}$	9.117 ± 0.065	N2/O2a	SF
17886	2007jh	0.29 ± 0.01	—	$(3.28 \pm 1.68) \times 10^{-2}$	N/A	caseX	N/A
18030	2007kq	70.34 ± 2.03	0.25 ± 0.05	$(3.20 \pm 0.06) \times 10^{-1}$	8.556 ± 0.052	N2/O2a	SF
18298	2007li	1.12 ± 0.26	—	$(2.07 \pm 0.33) \times 10^{-2}$	9.178 ± 0.073	N2/O2g	N/A
18612	2007lc	11.05 ± 0.13	0.58 ± 0.05	$(2.79 \pm 0.09) \times 10^{-1}$	9.044 ± 0.009	N2/O2a	AGN
18643	2007lv	0.39 ± 0.20	—	$(4.05 \pm 1.35) \times 10^{-2}$	N/A	caseX	N/A
18697	2007ma	27.28 ± 0.53	0.54 ± 0.06	$(3.28 \pm 0.06) \times 10^{-1}$	9.036 ± 0.026	N2/O2a	SF

Table 1—Continued

ID ^a	IAU name	EW (H α)	$E(B - V)$	SFR [$M_{\odot} \text{ yr}^{-1} \text{ kpc}^{-2}$]	$\log_{10}(\text{O}/\text{H})+12$	Calib ^b	Env ^c
18721	2007mu	0.00 ± -1.00	-0.05 ± 0.18	$(1.05 \pm 0.16) \times 10^{-1}$	N/A	caseX	N/A
18751	2007ly	0.11 ± 0.16	—	$(2.31 \pm 1.84) \times 10^{-3}$	N/A	N/A	N/A
18809	2007mi	0.36 ± 0.29	—	$(1.79 \pm 2.05) \times 10^{-2}$	N/A	N/A	N/A
18835	2007mj	0.92 ± 0.32	—	$(2.63 \pm 1.06) \times 10^{-2}$	9.116 ± 0.064	N2/O2g	N/A
18855	2007mh	16.68 ± 0.88	0.18 ± 0.17	$(1.33 \pm 0.06) \times 10^{-1}$	9.128 ± 0.041	N2/O2a	SF
18890	2007mm	0.12 ± 0.22	-1.31 ± 0.47	$(7.46 \pm 2.83) \times 10^{-3}$	N/A	N2/Hai	N/A
18903	2007lr	11.85 ± 0.47	0.64 ± 0.11	$(2.23 \pm 0.06) \times 10^{-1}$	9.108 ± 0.043	N2/O2a	SF
19155	2007mn	10.12 ± 0.04	0.46 ± 0.05	$(1.90 \pm 0.03) \times 10^{-1}$	8.933 ± 0.027	N2/O2a	SF
19353	2007nj	16.18 ± 0.51	0.59 ± 0.11	$(1.83 \pm 0.05) \times 10^{-1}$	8.985 ± 0.034	N2/O2g	N/A
19616	2007ok	44.96 ± 0.27	0.61 ± 0.01	$(1.08 \pm 0.01) \times 10^0$	9.061 ± 0.004	N2/O2a	SF
19626	2007ou	39.39 ± 0.67	0.45 ± 0.02	$(4.96 \pm 0.08) \times 10^{-1}$	8.961 ± 0.007	N2/O2a	SF
19794	2007oz	-4.42 ± 1.09	—	N/A	N/A	N/A	N/A
19969	2007pt	54.19 ± 0.74	0.33 ± 0.03	$(7.38 \pm 0.09) \times 10^{-1}$	9.044 ± 0.009	N2/O2a	SF
20064	2007om	6.43 ± 0.40	1.15 ± 0.37	$(1.51 \pm 0.08) \times 10^{-1}$	8.763 ± 0.088	N2/O2a	AGN
20208	2007qd	55.31 ± 2.46	0.18 ± 0.07	$(5.67 \pm 0.26) \times 10^{-1}$	8.817 ± 0.028	N2/O2a	SF
20420	2007qw	129.65 ± 1.76	0.08 ± 0.03	$(5.23 \pm 0.06) \times 10^{-1}$	8.424 ± 0.039	N2/O2a	SF
20528	2007qr	18.18 ± 0.51	0.59 ± 0.11	$(3.66 \pm 0.01) \times 10^{-1}$	9.042 ± 0.008	N2/O2a	SF
20625	2007px	14.01 ± 0.56	0.54 ± 0.12	$(1.82 \pm 0.06) \times 10^{-1}$	8.989 ± 0.045	N2/O2a	N/A
20718	2007rj	7.37 ± 0.25	0.42 ± 0.13	$(1.63 \pm 0.05) \times 10^{-1}$	9.066 ± 0.025	N2/O2a	AGN
20889	2007py	1.16 ± 0.69	—	$(1.28 \pm 0.84) \times 10^{-2}$	N/A	N/A	N/A
21034	2007qa	38.00 ± 0.60	0.40 ± 0.04	$(5.79 \pm 0.09) \times 10^{-1}$	9.054 ± 0.009	N2/O2a	AGN
21502	2007ra	11.32 ± 0.20	0.58 ± 0.07	$(4.90 \pm 0.09) \times 10^{-1}$	8.876 ± 0.015	N2/O2a	AGN
21510	2007sh	14.19 ± 0.52	0.30 ± 0.09	$(1.70 \pm 0.05) \times 10^{-1}$	9.168 ± 0.035	N2/O2a	SF
21669	2007rs	1.91 ± 0.20	—	$(5.72 \pm 0.69) \times 10^{-2}$	9.171 ± 0.035	N2/O2g	N/A
21766	2007rc	31.66 ± 0.99	0.37 ± 0.05	$(1.03 \pm 0.05) \times 10^0$	9.093 ± 0.005	N2/O2a	SF
22075	2007si	0.19 ± 0.19	—	$(1.01 \pm 0.87) \times 10^{-2}$	N/A	N/A	N/A

Note. — "N/A" is tagged for non detection and "—" for low S/N cases.

^aWe attached the same ID for the host galaxies as the SNe Ia

^bThe scheme to calibrate the gas phase metallicity. Detail is written in the text.

^cA type of host galaxies. SF stands for the star forming galaxy and AGN for the galaxies with AGN activities.

^dNo IAU names have been attached but identified as SNe Ia.

Table 2. Standard parameters

Datasets	N	α	β	M	rms
Sample without color cut					
EW H α	81	0.08 (0.02)	3.00 (0.09)	-19.11 (0.01)	0.187
- low ($< 12\text{\AA}$)	40	0.13 (0.03)	2.91 (0.11)	-19.18 (0.02)	0.192
- high ($> 12\text{\AA}$)	41	0.07 (0.03)	3.25 (0.17)	-19.08 (0.02)	0.162
SFR surface density	83	0.09 (0.02)	3.06 (0.09)	-19.11 (0.01)	0.188
- low ($< 1.1 \times 10^{-2} M_{\odot} \text{ yr}^{-1} \text{ kpc}^{-2}$)	41	0.13 (0.03)	3.03 (0.13)	-19.16 (0.02)	0.198
- high ($> 1.1 \times 10^{-2} M_{\odot} \text{ yr}^{-1} \text{ kpc}^{-2}$)	42	0.06 (0.03)	2.93 (0.15)	-19.09 (0.02)	0.167
metallicity	72	0.07 (0.02)	2.74 (0.09)	-19.09 (0.01)	0.177
- low ($\log_{10}(\text{O}/\text{H})+12 < 9.0$)	36	0.07 (0.03)	3.21 (0.16)	-19.07 (0.02)	0.189
- high ($\log_{10}(\text{O}/\text{H})+12 > 9.0$)	36	0.09 (0.03)	2.54 (0.11)	-19.12 (0.02)	0.138
Sample with $c_{salt} < 0.3$					
EW H α	73	0.09 (0.02)	2.53 (0.16)	-19.10 (0.01)	0.163
- low ($< 13\text{\AA}$)	36	0.14 (0.04)	2.38 (0.27)	-19.17 (0.02)	0.168
- high ($> 13\text{\AA}$)	37	0.07 (0.03)	2.49 (0.20)	-19.08 (0.02)	0.141
SFR surface density	73	0.10 (0.02)	2.53 (0.16)	-19.10 (0.01)	0.160
- low ($< 1.77 \times 10^{-1} M_{\odot} \text{ yr}^{-1} \text{ kpc}^{-2}$)	36	0.14 (0.03)	2.53 (0.23)	-19.14 (0.02)	0.176
- high ($> 1.77 \times 10^{-1} M_{\odot} \text{ yr}^{-1} \text{ kpc}^{-2}$)	37	0.06 (0.04)	2.39 (0.22)	-19.10 (0.02)	0.129
metallicity	67	0.09 (0.02)	2.35 (0.15)	-19.09 (0.01)	0.153
- low ($\log_{10}(\text{O}/\text{H})+12 < 9.0$)	33	0.08 (0.03)	2.41 (0.21)	-19.08 (0.02)	0.165
- high ($\log_{10}(\text{O}/\text{H})+12 > 9.0$)	34	0.11 (0.03)	2.28 (0.21)	-19.12 (0.02)	0.135

Note. — Standard parameters and a scatter of the Hubble residual are calculated to each sample for dependences on host characteristics: metallicity, SFR surface density and EW H α . Then each sample is halved by their host characteristics to examine a possible anomaly between the low and high subsamples. Uncertainties are listed within parenthesis.